Article

Current Biology

Autophagy Is Required for Memory Formation and Reverses Age-Related Memory Decline

Highlights

- Autophagy induction in hippocampal neurons is required to promote memory formation
- Hippocampal autophagy induction enhances activity-dependent synaptic plasticity
- Inducing autophagy in old hippocampi is sufficient to reverse age-impaired memory
- Autophagy integrates the effects of youthful systemic factors in the aged brain

Authors

Mélissa Glatigny, Stéphanie Moriceau, Manon Rivagorda, ..., Etienne Morel, Patrice Codogno, Franck Oury

Correspondence

patrice.codogno@inserm.fr (P.C.), franck.oury@inserm.fr (F.O.)

In Brief

Glatigny et al. show that autophagy induction in hippocampal neurons enhances cognition by promoting memory formation and integrating the effects of youthful systemic factors. During aging, hippocampal autophagy is reduced and its induction is sufficient to improve age-impaired memory.

Glatigny et al., 2019, Current Biology *29*, 435–448
February 4, 2019
https://doi.org/10.1016/j.cub.2018.12.021

CellPress

Current Biology
Article

Autophagy Is Required for Memory Formation and Reverses Age-Related Memory Decline

Mélissa Glatigny,[1,7] Stéphanie Moriceau,[1,7] Manon Rivagorda,[1,7] Mariana Ramos-Brossier,[1,8] Anna C. Nascimbeni,[2,8] Fabien Lante,[3] Mary R. Shanley,[4] Nadir Boudarene,[1] Audrey Rousseaud,[1] Allyson K. Friedman,[4] Carmine Settembre,[5] Nicolas Kuperwasser,[6] Gérard Friedlander,[2] Alain Buisson,[3] Etienne Morel,[2] Patrice Codogno,[2,*] and Franck Oury[1,9,*]
[1]INSERM U1151, Institut Necker Enfants-Malades (INEM), Team 14, Université Paris Descartes-Sorbonne—Paris Cité, 75014 Paris, France
[2]INSERM U1151, Institut Necker Enfants-Malades (INEM), Team 1, Université Paris Descartes-Sorbonne—Paris Cité, 75014 Paris, France
[3]Grenoble Institut des Neurosciences, INSERM U1216, Equipe Neuropathologies et Dysfonctions Synaptiques, Université Grenoble Alpes, Grenoble, France
[4]Department of Biological Sciences, City University of New York—Hunter College, 695 Park Avenue, New York, NY 10065, USA
[5]Department of Cell Biology and Disease Mechanisms, Telethon Institute of Genetics and Medicine, Naples, Italy
[6]INSERM U1151, Institut Necker Enfants-Malades (INEM), Team 5, Université Paris Descartes-Sorbonne—Paris Cité, 75014 Paris, France
[7]These authors contributed equally
[8]These authors contributed equally
[9]Lead Contact
*Correspondence: patrice.codogno@inserm.fr (P.C.), franck.oury@inserm.fr (F.O.)
https://doi.org/10.1016/j.cub.2018.12.021

SUMMARY

Age-related declines in cognitive fitness are associated with a reduction in autophagy, an intracellular lysosomal catabolic process that regulates protein homeostasis and organelle turnover. However, the functional significance of autophagy in regulating cognitive function and its decline during aging remains largely elusive. Here, we show that stimulating memory upregulates autophagy in the hippocampus. Using hippocampal injections of genetic and pharmacological modulators of autophagy, we find that inducing autophagy in hippocampal neurons is required to form novel memory by promoting activity-dependent structural and functional synaptic plasticity, including dendritic spine formation, neuronal facilitation, and long-term potentiation. We show that hippocampal autophagy activity is reduced during aging and that restoring its levels is sufficient to reverse age-related memory deficits. Moreover, we demonstrate that systemic administration of young plasma into aged mice rejuvenates memory in an autophagy-dependent manner, suggesting a prominent role for autophagy to favor the communication between systemic factors and neurons in fostering cognition. Among these youthful factors, we identify osteocalcin, a bone-derived molecule, as a direct hormonal inducer of hippocampal autophagy. Our results reveal that inducing autophagy in hippocampal neurons is a necessary mechanism to enhance the integration of novel stimulations of memory and to promote the influence of systemic factors on cognitive fitness. We also demonstrate the potential therapeutic benefits of modulating autophagy in the aged brain to counteract age-related cognitive impairments.

INTRODUCTION

In the mammalian brain, the hippocampus is pivotal for the control of learning and memory. The formation and consolidation of memory relies on the capacity of the hippocampus to integrate novel stimuli through neuronal structural reorganization and plasticity [1–4]. In hippocampal neurons, autophagosomes (APs), double-membraned vesicles involved in autophagy, have been shown to actively form in synapses and along neuronal processes [5–7], and emerging data suggest that hippocampal autophagy may contribute to neuronal homeostasis, playing a role in synaptic assembly, axonal growth, dopamine release, and long-term depression (LTD) [5–10].

Autophagy is a cellular catabolic process whereby proteins and organelles are engulfed in APs and then transported to lysosomes for degradation [11, 12]. The biogenesis of APs is orchestrated by multiple ATG (autophagy-related) proteins (such as beclin 1, Fip200, and VPS34) that are engaged in different dynamic membrane complexes [13–15]. The ATG5/12/16L1 complex finally allows for lipidation of the LC3 protein (LC3-II), which is then recruited to the site(s) of nascent APs to favor the maturation of the AP [13–15]. Beyond its basal functions, autophagy can be stimulated by various physiological stimuli and changes in environmental conditions [12]. There is now increasing evidence that autophagy induction is essential to control important physiological functions, such as regulation of energy metabolism, control of appetite, and modulation of host defenses, by mediating the cellular adaptive responses to novel physiological stimuli [12, 16, 17]. However, the role of this stimulated autophagy remains largely elusive in the brain. The fact that memory and neuronal plasticity in the hippocampus undergo changes in cellular protein homeostasis and organelle turnover [1, 18] and that hippocampal neurons are constantly subjected to novel stimuli and modulated by environmental factors leads us to

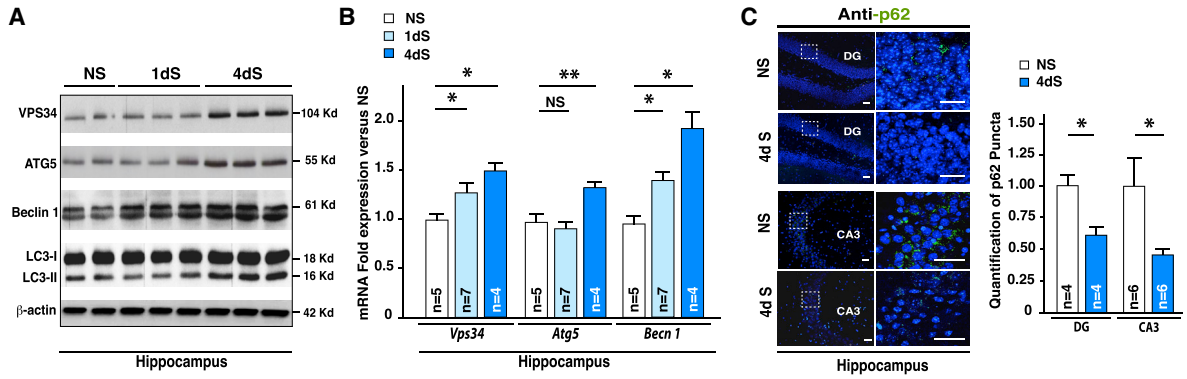

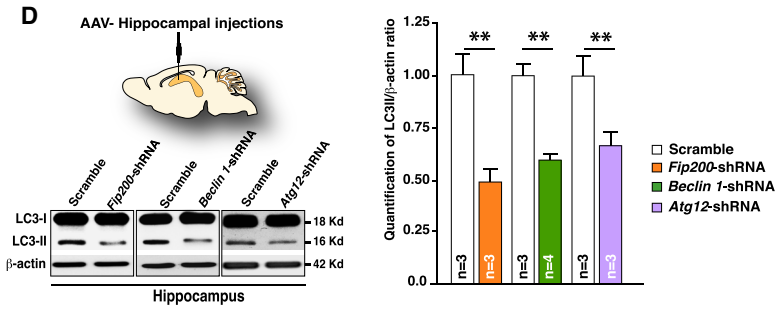

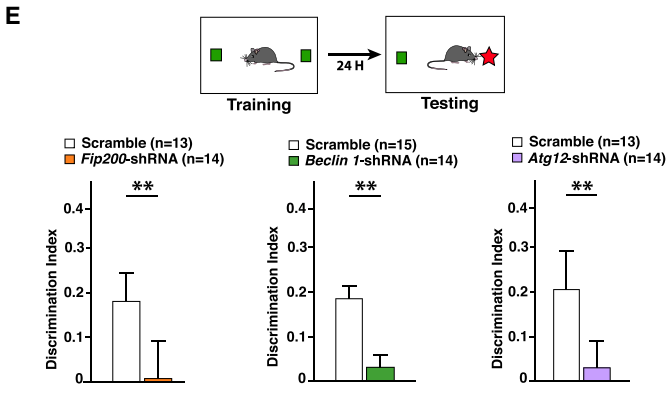

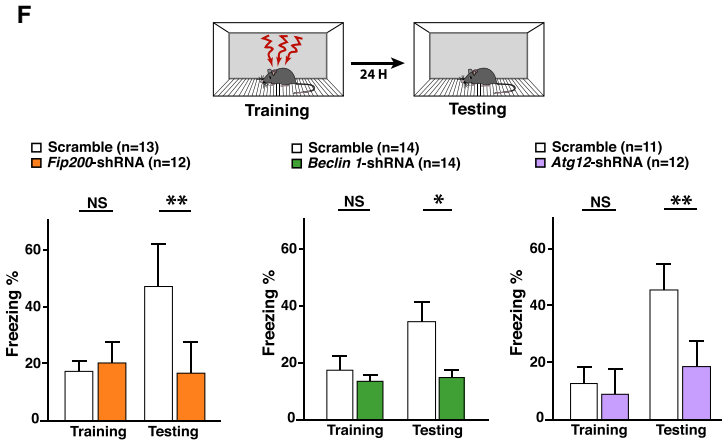

(legend on next page)

hypothesize that autophagy has an important functional role in regulating hippocampal-dependent cognitive fitness.

Importantly, the hippocampus is highly vulnerable to aging, exhibiting alterations in functional synaptic plasticity and progressive impairments in associated learning and memory [4, 19–23]. Given the current increase in life expectancy, the number of individuals affected by age-related memory loss is bound to dramatically increase and represents an unmet medical need [1, 24]. Recent progress has demonstrated the potential therapeutic effects of exposure to a "young" systemic milieu in preventing and/or reversing aging-associated memory decline, pointing to the importance of systemic circulating factors in the control of hippocampal cognitive fitness [25–28]; however, the mechanisms mediating this phenomenon in neurons are still poorly understood. Therefore, identification of intracellular mechanisms favoring neuronal plasticity and memory in the hippocampus is important in understanding how cognition and memory are affected during aging. Interestingly, the age-related decline in hippocampal-dependent memory is commonly associated with a reduction of ATG proteins in various tissues, including brain in which *Atg5*, *Atg7*, and *Becn 1* are found to be downregulated [29–31].

Given the above observations, we set out to determine the functional significance of autophagy in hippocampal-dependent cognitive fitness and to elucidate whether age-impaired autophagy in the brain is directly responsible for hippocampal-dependent memory deficits. We show that memory-related stimulations enhance autophagy activity in mouse hippocampi and that this induction is required to form novel memory by promoting the activity-dependent synaptic plasticity in hippocampal neurons. Furthermore, we show that autophagy activity is reduced in old hippocampi and that restoring its level fully reverses associative and spatial memory deficits in aged mice. In addition, we show that autophagy is induced in hippocampal neurons by exposure to a young systemic milieu and identify osteocalcin (Ocn) as one such circulating factor in young plasma. Together, these data demonstrate that the activation of autophagy by novel stimulations is necessary to promote the capacity of hippocampal neurons to form new memories and that young circulating factors improve cognitive performance in aged mice by inducing autophagy in the hippocampus. These results demonstrate the potential therapeutic benefits of promoting autophagy in aged brains to reverse and/or prevent the effects of aging on cognitive functions.

RESULTS

Hippocampal Autophagy Is Upregulated by Novel Stimulations of Memory

We first observed that exposing 3-month-old mice to novel memory-related stimulations, induced by contextual fear conditioning (CFC), enhanced the expression of key ATGs (beclin 1, VPS34, and ATG5) at both the mRNA and protein level in the hippocampus, and this upregulation was proportional to the level of stimulation (Figures 1A, 1B, and S1A). Similar results were obtained after exposing mice to Morris water maze tasks (MWM) (Figure S1C). Moreover, the increase in LC3-I conversion to LC3-II (AP formation marker) together with a decrease in SQSTM1/p62 (an AP cargo protein degraded after fusion with the lysosome) demonstrates that novel memory stimulations enhanced autophagic flux in the hippocampus (Figures 1A, 1C, S1B, S1D, and S1E). Although we cannot exclude that training itself induces autophagy in the hippocampal region of the brain, the fact that our control mice were subjected to the same context but without exposure to the memory paradigm indicates that novel memory-related stimulations induce hippocampal autophagy. Moreover, neither CFC nor MWM stimulations affect LC3-II abundance in the cerebellum (a brain region not directly implicated in the control of memory functions; Figures S1F and S1G). Lastly, exposing mice to acute restraint stress did not induce any modifications in hippocampal autophagy as seen after CFC or MWM (Figure S1H). Together, these data indicate that memory-related stimulations upregulate hippocampal autophagy and strongly suggest that autophagy plays a role in the regulation of learning and memory in the hippocampus.

Figure 1. Autophagy Is Upregulated in the Hippocampus by Novel Memory Stimuli and Promotes Learning and Memory

(A and B) VPS34, beclin 1, ATG5, LC3-I, and LC3-II accumulation (A; representative western blot) and *Vps34*, *Beclin 1* (*Becn 1*), and *Atg5* expression (B; qPCR performed in triplicate for each sample) in hippocampi of 3-month-old WT mice exposed to 1 (1dS) or 4 (4dS) consecutive days of memory-related stimulations induced by 3-foot-shock CFC. The hippocampi were collected 1 hr after the first (1dS; n = 7) or 1 hr after the last (4dS; n = 4–7) memory-related stimulation. The results are represented in comparison to 3-month-old WT mice exposed to the same context but without memory paradigm (NS; n = 5 or 6). β-actin was used as a loading control for each sample. Quantification of mRNA expression is relative to the NS group. These measurements were performed in two independent experiments for (A) and (B). See also Figure S1.

(C) SQSTM1/p62 immunofluorescence (scale bars represent 20 μm) performed on brain cross-sections at the level of the hippocampal dentate gyrus (DG) (n = 4) and CA3 regions (n = 6) in 3-month-old WT mice after 4dS of memory-related stimulation compared to the NS group. Brains were collected from two independent cohorts of mice for each group. See also Figure S1.

(D) LC3-I and LC3-II accumulation and LC3-II/β-actin ratio quantification in mouse hippocampi 3 weeks after stereotactic injections with either AAV-*Fip200*-shRNA (n = 3), AAV-*Beclin 1*-shRNA (n = 4), AAV-*Atg12*-shRNA (n = 3), or their respective AAV-Scramble-shRNA (n = 3 or 4). The quantification is relative to mice injected with AAV-Scramble. These measurements were obtained from 3 independent experiments for each group and its respective control. See also Figure S2.

(E) Novel object recognition (NOR) performed in 3-month-old mice 3 weeks after hippocampal stereotactic injections with either AAV-*Fip200*-shRNA (n = 14), AAV-*Beclin 1*-shRNA (n = 14), AAV-*Atg12*-shRNA (n = 14), or their AAV-Scramble-shRNA (n ≥ 10). Discrimination index was measured 24 hr after the training phase to assess memory performances. The NOR was performed in two independent experiments for each group and its respective control. See also Figure S2.

(F) 3-foot-shock contextual fear conditioning (CFC) performed in 3-month-old mice 3 weeks after stereotactic injections with either AAV-*Fip200*-shRNA (n = 12), AAV-*Beclin 1*-shRNA (n = 14), AAV-*Atg12*-shRNA (n = 12), or their AAV-Scramble-shRNA (n ≥ 10). Percent freezing was measured for the training (as a control for the basal level of mouse freezing) and testing phases (to assess memory performances). The CFC was performed in two independent experiments for each group and its respective control.

Independent cohorts of mice were used for each behavioral test (no mice were used in more than one behavioral test). Data are expressed as mean ± SEM. *$p \leq 0.05$; **$p \leq 0.01$; ***$p \leq 0.001$; NS, not significant, by Student's t test compared to the control group.

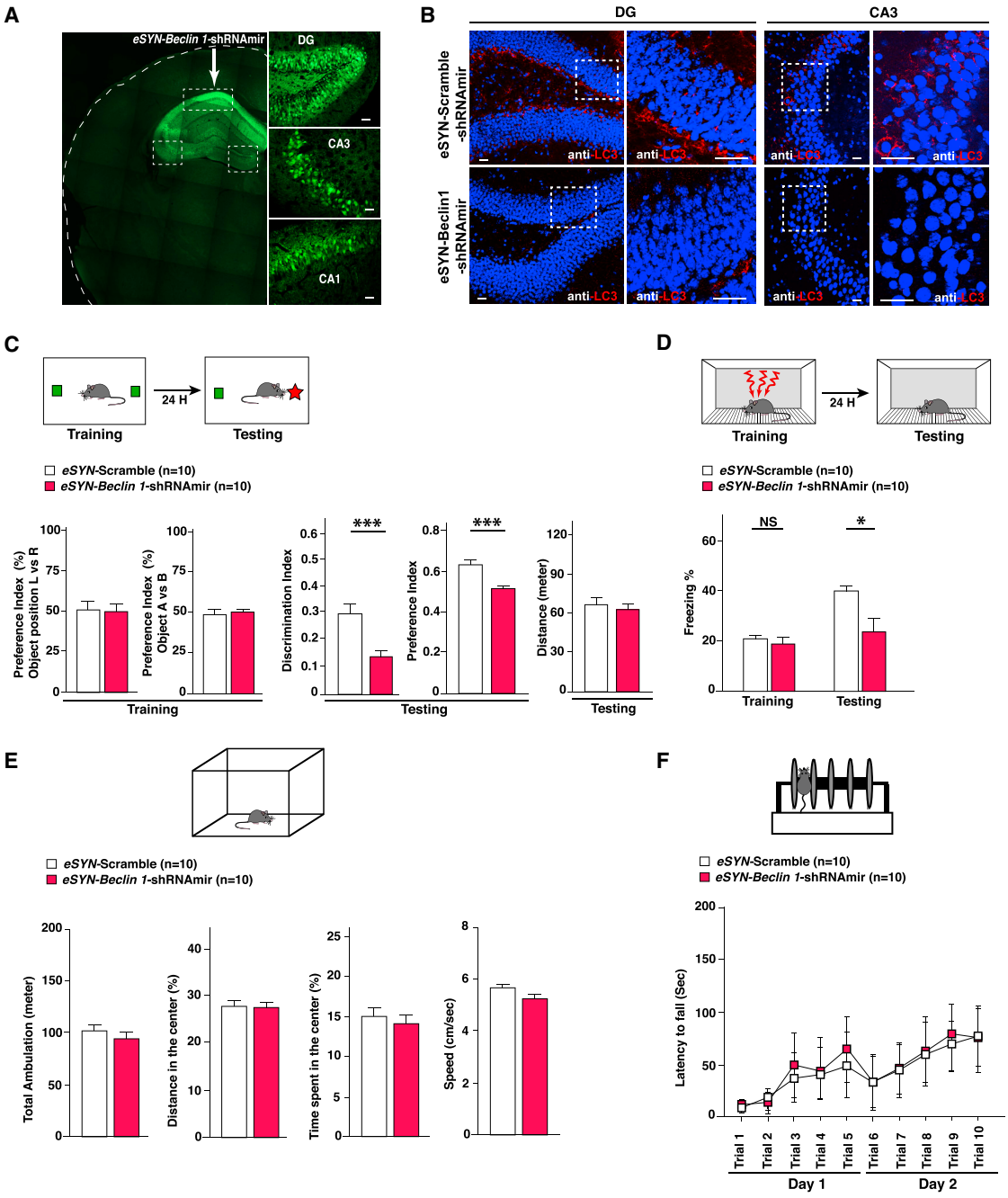

Figure 2. Selective Downregulation of Autophagy in Hippocampal Neurons Reduced Memory Performances

(A and B) Fluorescent microscopy images of brain cross-sections collected 3 weeks after local stereotactic injections with AAV-eSYN-Beclin 1-shRNAmir (shRNA driven by a synapsin 1 gene hybrid promoter).

(A) The construct expresses eGFP, which allows for verification of the site and efficacy of infection. The left panel is a panoramic photo of an entire brain region obtained by automatically aligning and stitching 54 tiled images into a mosaic (using the Zen Light Zeiss LSM software package). A focus was made on the Dentate Gyrus (DG), CA3 and CA1 regions of the hippocampus (right images).

(B) LC3 Immunofluorescence (Scale bar = 20μm) performed at the level of the dentate gyrus (DG) and CA3 of the hippocampus. The analysis was performed on n = 6 animals for each group derived from two independent cohorts of mice.

(C) NOR performed in 3-month-old mice, 3 weeks after hippocampal stereotactic injections with either AAV-eSYN-*Beclin 1*-shRNAmir (n = 10) or AAV-Scramble-shRNAmir (n = 10). Discrimination (3rd panel) and preference indexes (4th panel) were measured 24 hr after the training phase to assess memory performances. As control, preference index for the (right versus left) object location (1st panel) or for the object A versus B (2nd panel) during the training phase of the NOR was measured. We confirm that no initial preference for any exposed object (A or B) or any orientation (right versus left) was observed in any group. We also quantified the locomotion by measuring the distance (meter) traveled by each mouse group during the testing phase (5th panel), and no differences were observed. The NOR was performed in two independent experiments for each group and its respective control.

(legend continued on next page)

Neuronal Autophagy Influences Hippocampal-Dependent Memory Performances

To further investigate the functional significance of memory-induced autophagy, we generated mouse models to selectively downregulate hippocampal autophagy by performing stereotactic injections of adeno-associated viruses (AAV) expressing short hairpin RNAs (shRNAs) against *Fip200*, *Beclin 1*, or *Atg12*, major genes involved in distinct dynamic membrane complexes controlling different steps of AP biogenesis [14–16]. A decrease in the abundance of LC3-II and an increase of SQSTM1/p62 accumulation, observed 3 weeks after injections of each AAV, confirmed that autophagy was significantly hampered in the hippocampus (Figures 1D and S2A–S2H). Mice were then subjected to two independent behavioral tasks to assess hippocampal-dependent learning and memory [32]: the novel object recognition (NOR) test (Figures 1E and S2I–S2K) and the 3-foot-shocks CFC paradigm (Figure 1F). Both tests assess associative memory and rely on two phases: a training phase, in which mice are exposed to novel memory stimulations (NOR: exposure to two similar objects; CFC: 3 foot-shocks associated to a neutral environment) and a testing phase performed 24 hr after the training phase, in which memory performances are evaluated (NOR: recognition of a novel exposed object; CFC: measurement of context-elicited freezing). In NOR, we found that the downregulation of either *Fip200*, *Beclin 1*, or *Atg12* severely impaired memory capacities as demonstrated by a drastic decrease in the time exploring a novel object compared to control mice (Figures 1E and S2I–S2K). We next confirmed these results in CFC by showing that all mice downregulated for autophagy exhibited a decrease in freezing in contextual memory testing (Figure 1F). Importantly, the downregulation of *Beclin 1* selectively in hippocampal neurons, obtained after stereotactic AAV injections of a neuronal synapsin 1 promoter-driven shRNA for *Beclin 1* (eSYN-*Beclin 1*-shRNAmir) (Figures 2A and 2B), leads to similar memory deficits in NOR (Figure 2C) and CFC (Figure 2D) tests. Importantly, these mutant mice and their controls showed comparable performances in the open field (OFT) and rotarod tests, indicating that their locomotor functions and anxiety state were unaffected (Figures 2E and 2F).

Stimulation-Induced Autophagy in the Hippocampus Is Necessary to Form New Memories

The above results demonstrate that reducing autophagy in the hippocampus impairs cognitive fitness. As autophagy is acutely upregulated during exposure to novel memory-related stimuli, we hypothesized that autophagy plays a role specifically during novel stimulations in hippocampal neurons and consequently contributes to the formation of new memories. Therefore, we acutely targeted hippocampal autophagy during exposure to novel stimulations (training phase) or after the training phase by performing single hippocampal stereotactic injections of pharmacological inhibitors of autophagy using spautin-1 (specific autophagy inhibitor-1, which interferes with AP formation) or by blocking the late stages of the autophagic pathway by using leupeptin or chloroquine (Figures 3A and S3A–S3F). The acute reduction of hippocampal autophagy activity after injections of pharmacological autophagy inhibitors was confirmed by measuring LC3-II abundance (Figures 3A and S3A–S3C) and SQSTM1/p62 (Figures S3E and S3F) levels. When autophagy is acutely inhibited during the training phase of either the NOR or CFC, we found significant decreases in memory performances during testing in both behavioral tests (Figures 3B–3D and S4A–S4F). Conversely, acute induction of autophagy by hippocampal injections of TAT-beclin 1 peptide [33], an inducer of AP formation, during the training phases, enhanced memory capacities in both the NOR and CFC tests compared to control groups (vehicle or TAT-scramble-injected mice; Figures 3B–3D and S4D–S4F). Importantly, modulating autophagy 12 hr after exposure to novel stimulations with either spautin-1, leupeptin, or TAT-beclin 1 (Figure 3E) did not influence memory performances in both tests (Figures 3F, 3G, S4G, and S4H), showing that stimulation-induced autophagy in the hippocampus is specifically required during the formation of novel memories.

Stimulation-Induced Autophagy Enhances Activity-Dependent Structural and Functional Synaptic Plasticity in Hippocampal Neurons

In order to gain insight into the neuronal consequences of hippocampal stimulation on autophagy, we isolated primary hippocampal neurons from mice and subjected them to stimulation by chemical depolarization with potassium chloride (KCl) or chemical long-term potentiation (cLTP), a putative functional correlate of learning and memory that has been shown to induce synaptic plasticity [34, 35]. As shown in Figure 4A, both KCl and cLTP treatments enhanced AP formation as determined by measuring LC3-II levels. In addition, as previously described [34, 35], we observed that cLTP treatment also increased dendritic spine formation and enhanced GluA1 and CAMKIIα phosphorylation, markers of increased synaptic strength (Figures 4C and 4D). Therefore, we next investigated whether downregulation of autophagy affected these structural and molecular changes. We observed that the acute downregulation of *Beclin 1* in primary hippocampal neurons (Figure 4B) blocks the formation of novel dendritic spines and phosphorylation of GluA1 and

(D) CFC performed in 3-month-old mice 3 weeks after stereotactic injections with either AAV-eSYN-*Beclin 1*-shRNAmir (n = 10) or AAV-Scramble-shRNAmir (n = 10). Percent freezing was measured for the training and testing phases. The CFC was performed in two independent experiments for each group and its respective control.

(E) Open field test (OFT) performed in 3 month old, 3 weeks after hippocampal stereotactic injections with either AAV-eSYN-*Beclin 1*-shRNAmir (n = 10) or AAV-Scramble–shRNAmir (n = 10). Total ambulation (meter), distance and time spent in the center of the arena (%), and speed (cm/s) were measured. This analysis was performed on 1 cohort of mice for each group.

(F) Rotarod test performed in 3 month old, 3 weeks after hippocampal stereotactic injections with either AAV-eSYN-*Beclin 1*-shRNAmir (n = 10) or AAV-Scramble-shRNAmir (n = 10). Values represent mean latency to fall during the 10 acquisition trials performed over 2 days (5 trials/day). This analysis was performed on 1 cohort of mice for each group.

Independent cohorts of mice were used for each behavioral test (no mice were used in more than one behavioral test). Data are expressed as mean ± SEM. *$p \leq 0.05$; **$p \leq 0.01$; ***$p \leq 0.001$; NS, not significant by Student's t test compared to control groups.

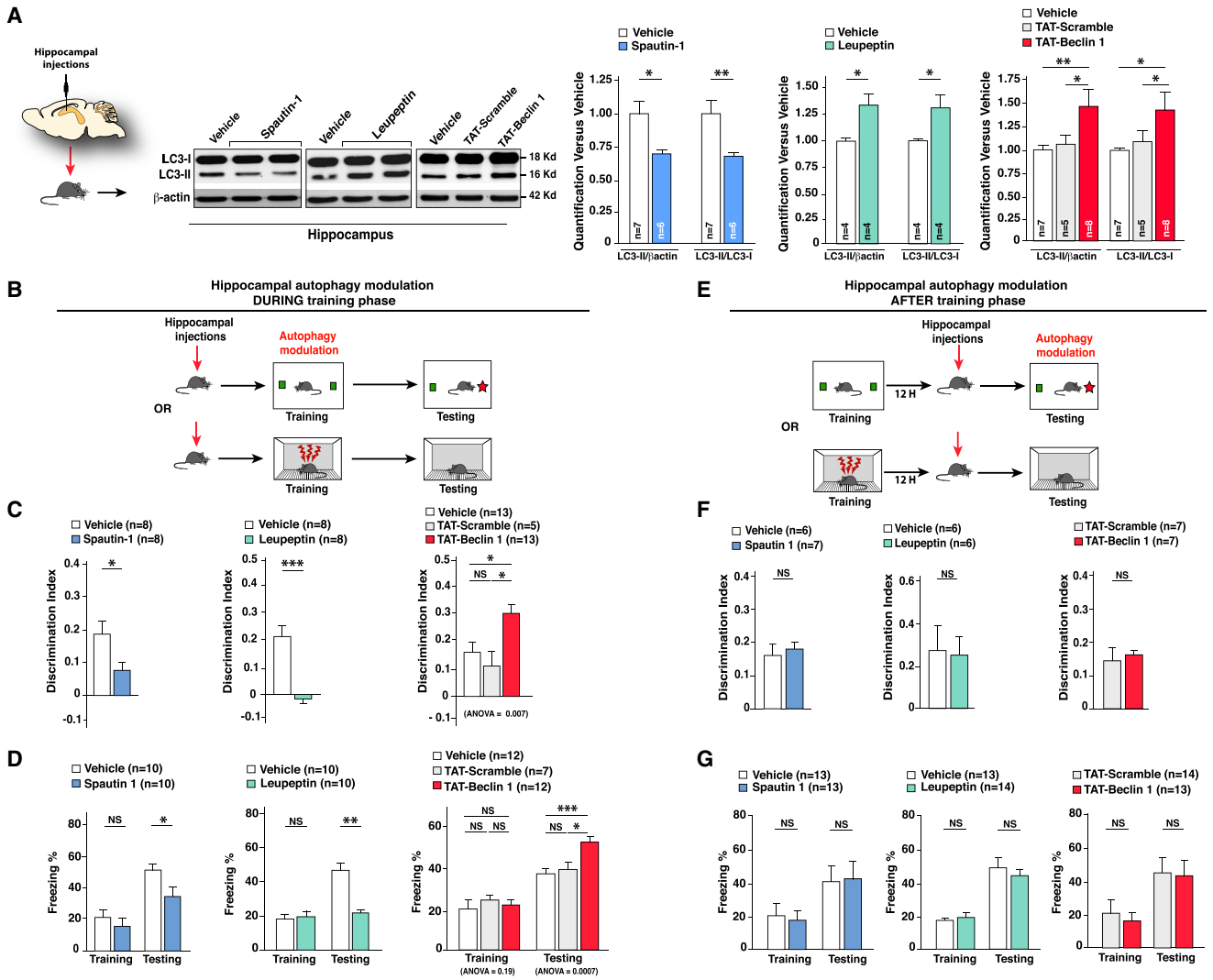

Figure 3. Induction of Autophagy in the Hippocampus Is Required to Form Novel Memory

(A) LC3-I and II accumulation (representative western blot, left) and quantification data (LC3-II/β-actin and LC3-II/LC3-I ratios, right) in 3-month-old mouse hippocampi 12 hr after stereotactic injections of either spautin-1 (5 μg/hemisphere; n = 6), leupeptin (100 ng/hemisphere; n = 4), TAT-Scramble (1 μg/hemisphere; n = 5), TAT-beclin 1 (1 μg/hemisphere; n = 8), or their respective vehicle (n ≥ 4). β-actin was used as a loading control for each sample. These measurements were obtained from two independent cohorts of mice for each treatment and its respective control. See also Figure S3.

(B) Schematic representation of the experimental procedure to induce a modulation of autophagy during the training phase (phase of novel memory-related stimulations). The training phase was performed 12 hr after hippocampal stereotactic injections of either spautin-1, TAT-Scramble, TAT-beclin 1, leupeptin, or their respective vehicles. Mice were subjected to the training phase of either NOR or CFC and then 24 hr later to the testing phase to assess memory performances. See also Figure S4.

(C and D) NOR (C) and CFC (D) performed in 3-month-old mice modulated for autophagy during the training phase following stereotactic injections with either spautin-1 (n = 8–10), leupeptin (n = 8–10), TAT-Scramble (n = 5–7), TAT-beclin 1 (n = 13 or 12), or their respective vehicle (n ≥ 8). For NOR, the discrimination index was measured for each group during the testing phase. For CFC, percent freezing was measured for each group during the training phase and testing phases to assess memory performances. The CFC was performed in two independent experiments for each treatment and its respective control. The NOR was performed on one cohort of mice for each treatment and its respective control. See also Figure S4.

(E–G) Schematic representation of the experimental procedure to induce a modulation of autophagy after the acquisition phase (E). 12 hr after training phase, mice were injected in the hippocampus with either spautin-1 (n = 7–13), leupeptin (n = 6–14), TAT-beclin 1 (n = 7–13), or their respective vehicle (n ≥ 6). Mice were then subjected, 12 hr later, to the testing phase of either NOR (F) or CFC (G). For NOR, the discrimination index was measured for each group during the testing phase. For CFC, percent freezing was measured for each group during the training and testing phases. The CFC was performed in two independent experiments for each treatment and its respective control. The NOR was performed on one cohort of mice for each treatment and its respective control. See also Figure S4. Independent cohorts of mice were used for each behavioral test (no mice were used in more than one behavioral test). Data are expressed as mean ± SEM. *p ≤ 0.05; **p ≤ 0.01; ***p ≤ 0.001; NS, not significant by Student's t test compare to WT mice injected with vehicle and (TAT-Beclin injections) by two-way ANOVA repeated-measure followed by a post hoc Tuckey's honestly significant difference (HSD) multiple comparisons test for pairwise differences between each group of mice.

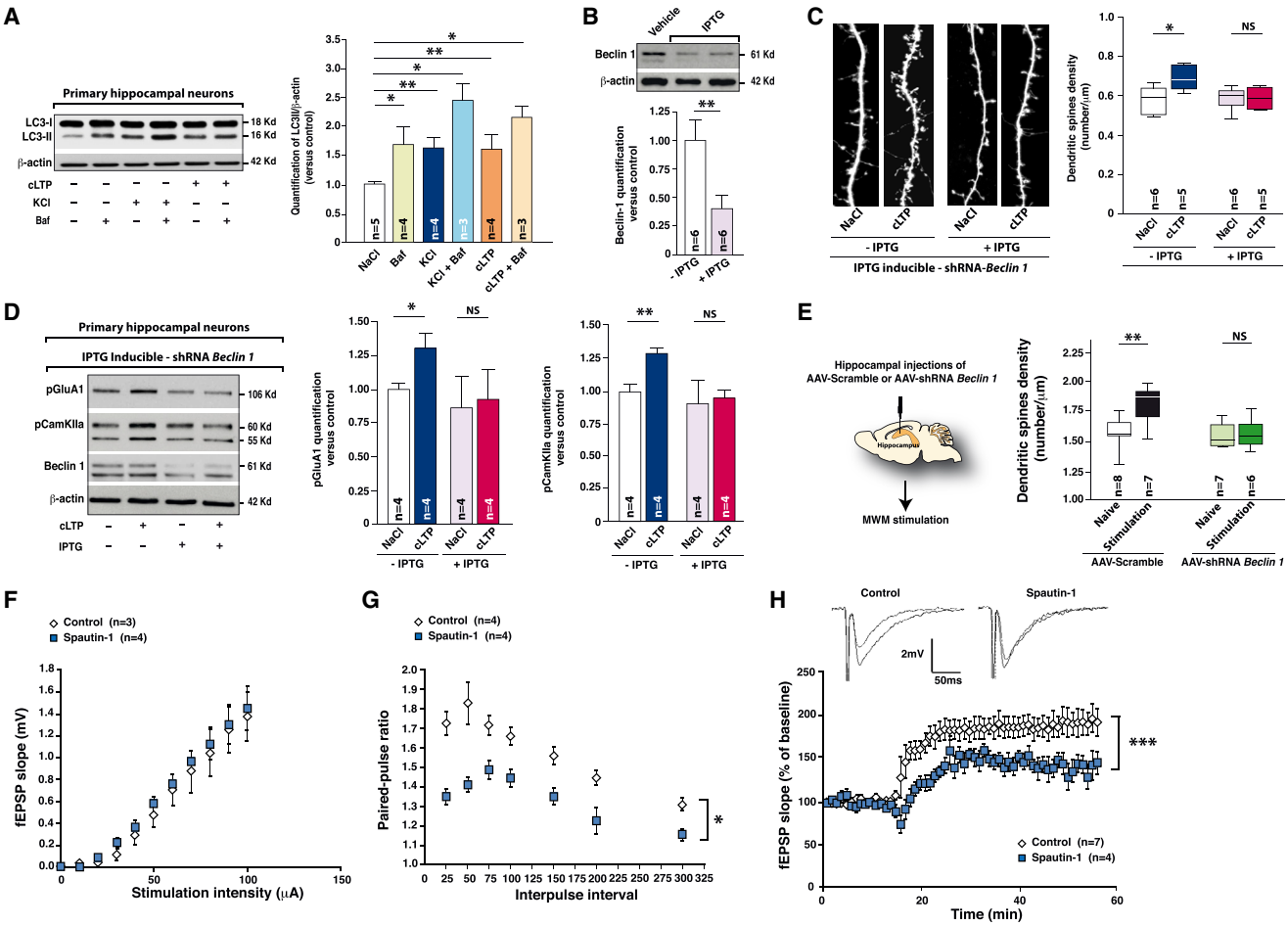

Figure 4. Autophagy Induction Is Necessary to Enhance Structural and Functional Activity-Dependent Synaptic Plasticity in Hippocampal Neurons

(A) LC3-I and II accumulation (representative western blot, left) and quantification data (LC3-II/β-actin ratio, right) in mature primary hippocampal neurons treated with either NaCl, bafilomycin A1 (Baf), KCl, KCl + Baf, chemical long-term potentiation (cLTP) or cLTP + Baf. The upregulation observed after adding Baf suggests an effect of KCl and cLTP on the induction of the AP formation. The quantification is represented in comparison to the vehicle-treated group (NaCl). β-actin was used as a loading control for each sample, and these measurements were obtained from n = 3 individual hippocampal neuronal preparations.

(B) Western blot analysis and quantification of beclin 1 in primary hippocampal neurons infected with lentiviruses expressing isopropyl β-D-1-thiogalactopyranoside (IPTG)-inducible *Beclin 1*-shRNA. The expression of *Beclin 1*-shRNA was induced with IPTG treatment. β-actin was used as a loading control for each sample. These measurements were obtained from n = 3 individual hippocampal neuronal preparations.

(C) Representative images and quantification of dendritic spines density (number of spines per μm) after NaCl or cLTP treatment of primary hippocampal neurons. These neurons were previously transfected with IPTG-inducible *Beclin 1*-shRNA and treated with either IPTG or vehicle. This analysis was performed on n = 5 experimental replicates; n ≥ 6 individual hippocampal neurons per group were evaluated for each experimental replicate (each individual hippocampal neuronal preparations derived from 12 different embryonic hippocampi).

(D) Western blot analysis (left) and quantification of band intensities (right) of the phosphorylated forms of GluA1 (pGluR1) and CaMKII (pCaMKIIa) in primary hippocampal neurons stimulated with either NaCl or cLTP. The neurons were previously infected with lentiviruses expressing IPTG-inducible *Beclin 1*-shRNA. The expression of *Beclin 1*-shRNA was induced with IPTG treatment (over 72 hr). β-actin was used as a loading control for each sample. These measurements were obtained from n = 4 individual hippocampal neuronal preparations.

(E) Measurement of dendritic spines density in hippocampal granule cells of the DG region in 3-month-old mice previously injected in the hippocampus with either AAV-*Beclin 1*-shRNA or AAV-Scramble-shRNA. The mice were subjected to novel memory-related stimulations induced by 5 consecutive days of Morris water maze (MWM) task. The measurement of dendritic spines density was performed on hippocampi of n ≥ 6 animals per group (n ≥ 8 individual neurons were evaluated per hippocampus). These measurements were obtained from 2 independent cohorts of mice for each group.

(F–H) Electrophysiological analyses of short- and long-term synaptic plasticity in the hippocampus (CA1 region) after acute autophagy inhibition.

(F) Basic synaptic transmission. The input-output curves were generated by computing stimulation intensity against field EPSP slope in control slices versus slices exposed to spautin-1 at 10 μM. Data were obtained on 7 slices from n = 4 mice in the control condition and 6 slices from n = 3 mice after spautin-1 treatment). I/O curves revealed no differences between the 2 groups of slices (p = 0.78).

(G) Paired pulse facilitation (PPF) of synaptic transmission. Data were obtained from 8 control slices from n = 4 mice and 8 spautin-1 treated slices from n = 4 mice. PPF was significantly decreased in slices treated with spautin-1 at 10 μM (p = 0.017; Mann-Whitney test).

(H) Long-term potentiation of synaptic transmission. Data were obtained from 7 control slices from n = 7 mice and 7 spautin-1 exposed slices from n = 4 mice. Representative traces from one experiment are shown on the top of the graph. Results show a significant decrease of LTP in slices perfused with spautin-1 at

(legend continued on next page)

CAMKIIα after cLTP treatment (Figures 4C and 4D), suggesting that autophagy induction is required to enhance the activity-dependent plasticity changes in hippocampal neurons during stimulation. Importantly, without neuronal stimulations, acutely targeting autophagy does not alter baseline levels of dendritic spine density or synaptic plasticity markers. To corroborate these structural results *in vivo*, we assessed dendritic spine density in mice that were locally injected with either AAV-*Beclin 1*-shRNA or AAV-Scramble-shRNA and subjected to MWM tasks (for 5 consecutive days), which is known to enhance dendritic spines formation in granular neurons of the hippocampal dentate gyrus (DG) [36, 37]. Results from Golgi staining revealed a significant induction of dendritic spine formation in DG hippocampal granular neurons of control mice, but not in mice that were downregulated for *Beclin 1* (Figure 4E). We then assessed the effect of acute autophagy inhibition (after treatment with spautin-1) on basal glutamatergic transmission and on short- and long-term plasticity in wild-type (WT) hippocampal slices. As shown on Figure 4F, the basal glutamatergic neurotransmission, defined by input-output (I/O) curves, was not significantly affected by acute treatment with spautin-1. In contrast, we observed a significant and sustained reduction of the paired-pulse facilitation ratio (PPF) in the slices treated with spautin-1, demonstrating a strong alteration of short-term plasticity mechanisms by acute autophagy inhibition (Figure 4G). Similarly, treatment with spautin-1 induced a significant decrease in LTP amplitude (Figure 4H). Indeed, the mean values of the field excitatory postsynaptic potential (fEPSP) slopes (measured during 10 min before the end of recordings) were significantly decreased in slices exposed to spautin-1 (190.66% ± 15.07% in control condition compared to spautin-1 139.37% ± 13.19%). These data demonstrate that autophagy is required to promote both structural and functional (short- and long-term) synaptic plasticity in hippocampal neurons in response to novel neuronal stimulations.

Promoting Autophagy in Old Hippocampi Is Sufficient to Reverse Age-Impaired Memory

Normal aging is characterized by a decline in hippocampal neuronal plasticity and increased memory impairments [4, 20–22] and is associated with a reduction of autophagy in various tissues [29–31]. In the hippocampi of 16-month-old mice, we observed a marked decrease in beclin 1, VPS34, and ATG5 at both the protein (Figures 5A and S5A) and mRNA level (Figure 5B). Furthermore, a reduction in autophagy activity was observed, as demonstrated by a slight decrease in LC3-II accumulation (Figure 5A), together with an increase in SQSTM1/p62 levels (Figures 5C and S5B). Co-immunofluorescence analysis indicates that the increase in SQSTM1/p62 puncta accumulation is highly present in neurons ($NeuN^+$ cells) but also in some astrocytes ($GFAP^+$ cells), both in the DG and CA3 regions of old hippocampi (Figure S5C). These results prompted us to examine whether inducing autophagy in old hippocampi could improve age-impaired memory deficits observed in 16-month-old mice (Figure 5D). To that end, we subjected 3- or 16-month-old WT mice to object location memory (OLM) (assessing spatial memory; Figure S5D), NOR (Figures 5E and S5E), and CFC (Figure 5F) tests after hippocampal stereotactic injections of TAT-beclin 1, TAT-Scramble, or vehicle. We observed that TAT-beclin 1 injections in 16-month-old animals induced autophagy and improved memory performances in all behavioral tests (Figures 5E, 5F, S5D, and S5E). These results indicate that promoting autophagy in old hippocampi is sufficient to rejuvenate memory in aged animals and suggests that hippocampal and/or organism changes contribute to reduced autophagy in the brain during aging.

Young Plasma Injections Reverse Aged-Memory Deficits by Promoting Autophagy in Old Hippocampi

Recent studies have shown that repeated systemic administrations of young blood plasma into aged animals improved age-related cognitive impairments by rehabilitating synaptic plasticity capacity [25–28]. This led us to investigate whether autophagy promotes the beneficial effects of young plasma on memory decline in aged mice. We found that 16-month-old mice that received plasma collected from young (8-week-old) mice had an increase of LC3-II accumulation and a slight decrease of SQSTM1/p62 levels in comparison to old mice that received vehicle (Figures 6A and S6A). Conversely, we did not detect differences in aged mice treated with aged plasma (from 16-month-old mice; Figures 6A and S6A). Subsequently, in an independent cohort of aged mice, we confirmed that systemic injections of young plasma reversed age-related memory deficits, but importantly, this reversal was not observed in 16-month-old animals in which *Beclin 1* was downregulated (Figures 6B and S6B). These data suggest that rejuvenating circulating factors present in young plasma ameliorate age-related memory deficits via restoring autophagy levels in old hippocampi.

Osteocalcin Is a Youthful Plasma Factor Inducing Hippocampal Autophagy in Old Mice

Interestingly, Ocn was recently identified as a necessary circulating factor of young plasma, which can rejuvenate hippocampal-dependent memory functions in aged mice [28, 38]. Ocn is a bone-derived hormone that crosses the blood-brain barrier, that influences hippocampal-dependent memory through the activation of its receptor Gpr158 in hippocampal neurons [28, 38–41], and its circulating levels are drastically reduced during aging [41, 42]. Importantly, we observed that Ocn treatment in primary hippocampal neurons significantly enhances AP formation, as shown by measuring LC3-II levels in the presence and in the absence of lysosomal blockers (bafilomycin), respectively (Figure 6C). This observation together with the fact that restoring its levels in 16-month-old mice is sufficient to reverse age-related cognitive impairments [28] prompted us to test whether Ocn ameliorates age-related memory deficits by increasing autophagy levels in old hippocampi. This question

10 μM ($p \leq 0.0001$; Mann-Whitney U test). All results were represented according to the number of animals used for each electrophysiological analyses represented in (F)–(H).

Results are given as mean ± SEM. *$p \leq 0.05$; **$p \leq 0.01$; ***$p \leq 0.001$; NS, not significant by Student's t test (A–E) or by non-parametric Mann-Whitney test (F–H) compared to control group.

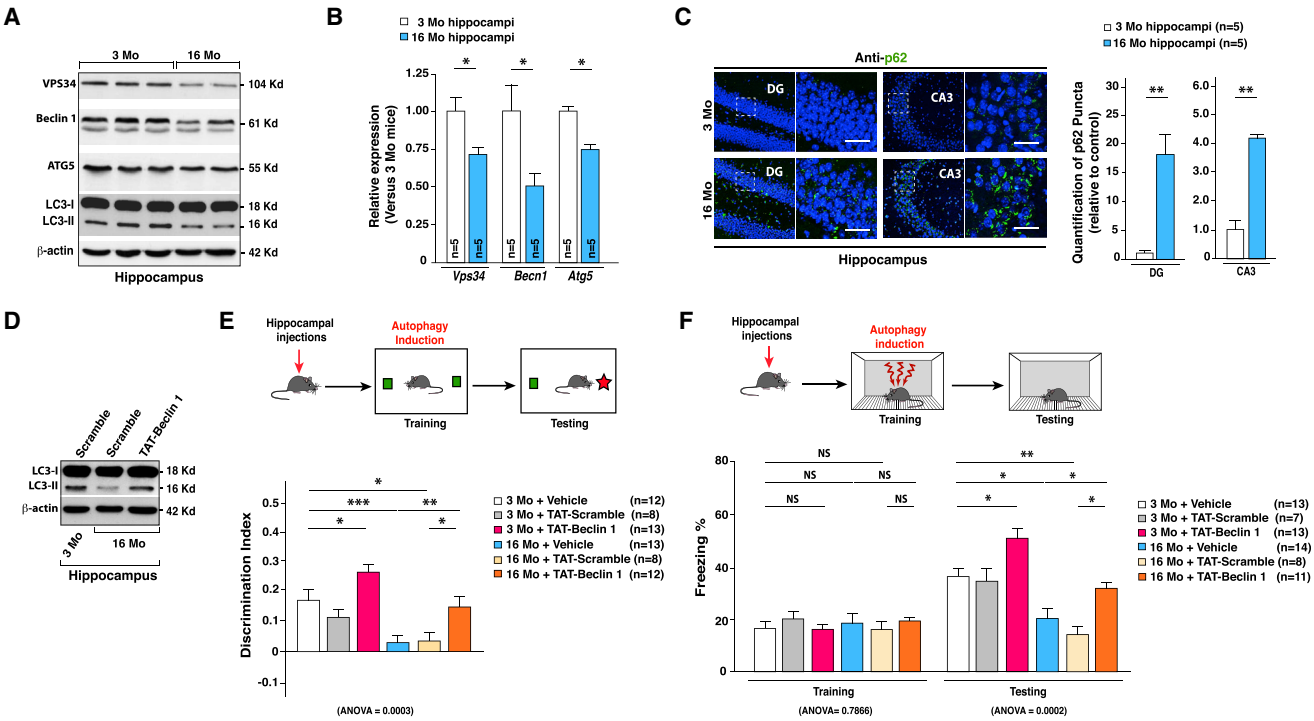

Figure 5. Promoting Hippocampal Autophagy Levels in Old Mice Is Sufficient to Reverse Age-Related Memory Deficits

(A) VPS34, beclin 1, ATG5, and LC3-I and II accumulation (representative western blot) in 3- (n = 5) or 16-month-old mouse (n = 5) hippocampi. β-actin was used as a loading control for each sample. These measurements were obtained from two independent cohorts of mice for each group. See also Figure S5.

(B) *Vps34*, *Becn 1* (*Beclin 1*), and *Atg5* relative expression (qPCR performed in triplicate) in the hippocampus of 3- (n = 5) or 16-month-old mice (n = 5). Quantification of mRNA expression is relative to 3-month-old mice.

(C) SQSTM1/p62 immunofluorescence (scale bars represent 20 μm) and puncta quantification performed on brain cross-sections, at the level of the hippocampal DG and CA3 regions of 3- (n = 5) and 16-month-old mice (n = 5). Quantification was performed relative to 3-month-old mice. These measurements were obtained from two independent cohorts of mice for each group. See also Figure S5.

(D) LC3-I and II accumulation 12 hr after hippocampal stereotactic injections of either TAT-Scramble (1 μg/hemisphere) or TAT-beclin 1 (1 μg/hemisphere) in 3- (n = 6) and 16-month-old mice (n = 6). β-actin was used as a loading control for each sample. This analysis was performed in 3 independent experiments. See also Figure S5.

(E) NOR performed in 3- and 16-month-old mice 12 hr after hippocampal stereotactic injections with either vehicle (n = 12 or 13), TAT-Scramble (n = 8), or TAT-beclin 1 (n = 13 or 12). Discrimination index was measured for each group during the testing phase. The NOR was performed in two independent experiments for each group of mice. See also Figure S5.

(F) CFC performed in 3- and 16-month-old mice 12 hr after hippocampal stereotactic injections with either vehicle (n = 13 or 14), TAT-Scramble (n = 7 or 8), or TAT-beclin 1 (n = 13–11). Percent freezing was measured in CFC for each group during the training and testing phases. The CFC was performed in two independent experiments for each group of mice. See also Figure S5.

Independent cohorts of mice were used for each behavioral test (no mice were used in more than one behavioral test). Results are given as mean ± SEM. *$p \leq 0.05$; **$p \leq 0.01$; ***$p \leq 0.001$; NS, not significant by Student's t test compared to 3-month-old mice injected with vehicle or TAT-Scramble and (E and F) by two-way ANOVA repeated-measure followed by a post hoc Tuckey's HSD multiple comparisons test for pairwise differences between each group of mice.

was addressed by two independent experiments. First, we show that hippocampal Ocn injections improved the enfeeblement of autophagy activity observed in 16-month-old hippocampi, as demonstrated by measuring LC3-II and SQSTM1/p62 protein levels (Figures 6D and S6C). Subsequently, we show that the contribution of Ocn is required to promote the effects of young plasma injections on age-impaired LC3-II levels. Indeed, injections of plasma from young WT mice immunodepleted for Ocn (90% of Ocn was reduced after immunodepletion; see STAR Methods) [28] failed to improve the decrease in LC3-II accumulation and the increase in SQSTM1/p62 levels in old mice to the same extent as the injections of young plasma control (treated with immunoglobulin G [IgG]; Figures 6E and S6D). Finally, we confirmed that systemic infusions of exogenous Ocn in 16-month-old mice improved age-related memory deficits. However, this Ocn-induced memory improvement was abolished in the hippocampal neurons of 16-month-old animals in which *Beclin 1* had been selectively downregulated (Figures 6F, S6E, and S6F). These data support the necessary contribution of autophagy in promoting the beneficial effects of young circulating factors on age-related memory decline and identify Ocn as a direct hormonal inducer of autophagy in hippocampal neurons. In total, these results demonstrate the importance of inducible hippocampal autophagy for cognitive fitness, especially during aging.

DISCUSSION

The identification of intracellular cues in hippocampal neurons that control memory formation is of utmost importance in order

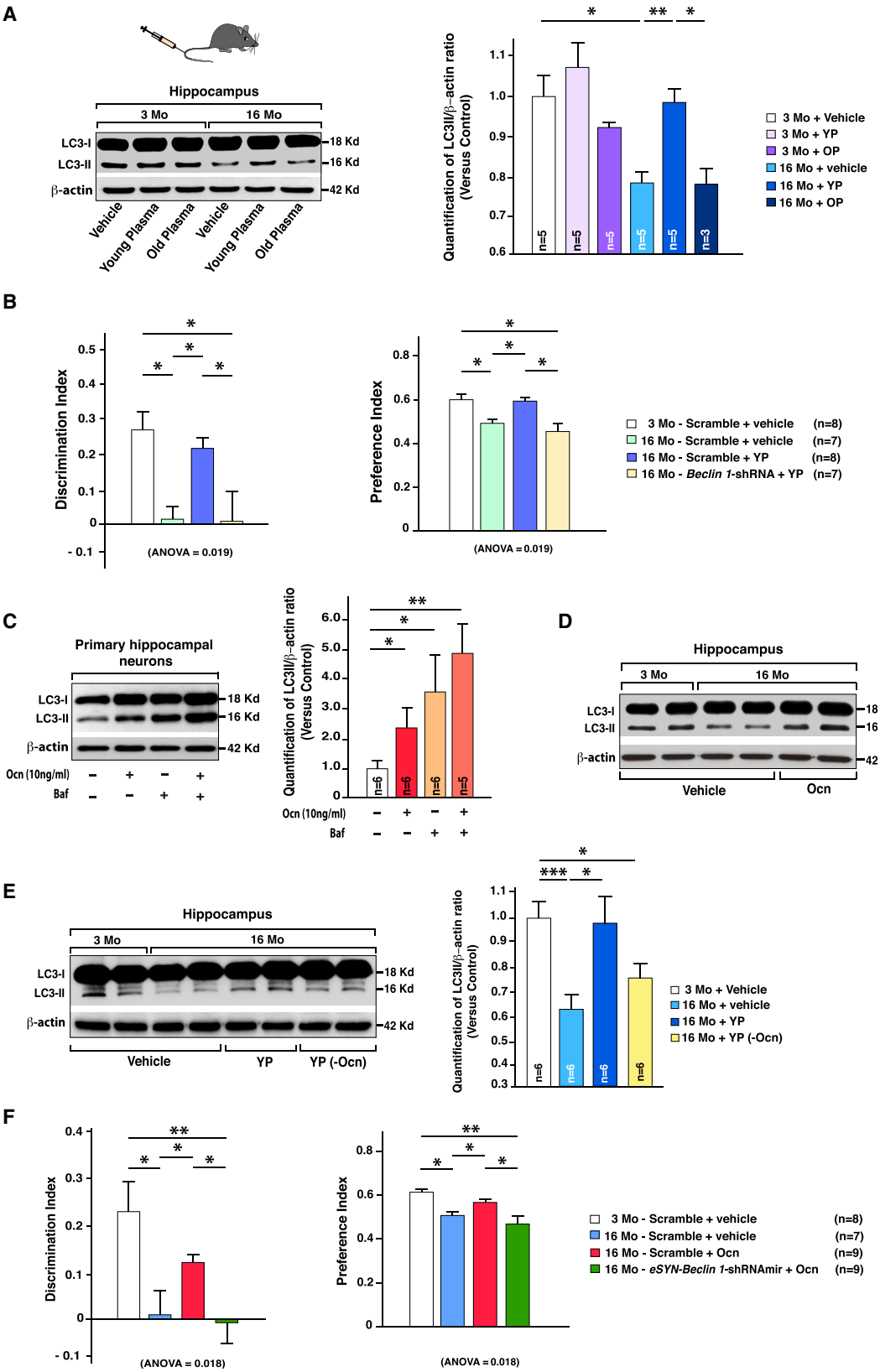

(legend on next page)

to understand how cognition is regulated and how it is altered under pathological and aging conditions. We show that the stimulation of memory by behavioral tasks upregulates autophagy in the hippocampus and that learning and memory is dependent on induced autophagy activity in hippocampal neurons. Next, we demonstrate that memory is influenced if autophagy is modulated during the training phases of behavioral tasks, when animals are exposed to novel stimulations. This suggests that neuronal stimulation induces an autophagic response that allows neurons in the hippocampus to incorporate these stimuli by promoting the formation of dendritic spines and increased synaptic strength. It is still unclear how neuronal stimulation induces an increase in autophagy levels; however, these results reveal an important physiological function of autophagy in the brain beyond its known cellular roles in housekeeping pathways. Our findings suggest autophagy promotes memory formation by modulating the adaptive responses of hippocampal neurons to novel stimuli.

Mechanistically, we show that autophagy induction is required for shaping activity-dependent synaptic plasticity in hippocampal neurons, including the enhancement of dendritic spine formation and synaptic molecular strength after stimulations. Nevertheless, our investigation did not allow us to determine dendritic spine type and morphology or whether these defects predominantly concern a specific neuronal population in the hippocampus. Electrophysiological analyses of brain slices following acute hippocampal autophagy inhibition suggested that basal neurotransmission was not affected. However, our data show a significant reduction in the amplitude of the field EPSP following LTP stimulation. This observation suggests that hippocampal autophagy is important for promoting long-term synaptic plasticity. Interestingly, age-dependent alterations in the induction of LTP are well documented [4]. Moreover, our electrophysiological findings also demonstrate that inhibiting autophagy acutely on hippocampal slices also induced a sustained reduction of the neuronal facilitation, namely PPF, a form of short-term activity-dependent synaptic plasticity. Changes in PPF observed after autophagy inhibition suggest a presynaptic involvement of autophagy in hippocampal neurons. Importantly, these findings can be corroborated with recent reports showing that presynaptic domains are active sites for AP biogenesis [5–7, 43, 44], suggesting an intimate dialogue between presynaptic domains and autophagy machinery. Finally, defects in neuronal facilitation may also contribute to postsynaptic alterations (i.e., a decrease in LTP amplitude). Together, these findings indicate that acute downregulation of hippocampal autophagy does not affect basal neurotransmission but reduces both short- and long-term activity-dependent synaptic plasticity capacity in hippocampal neurons in response to novel neuronal stimuli.

The selective downregulation of beclin 1 in hippocampal neurons and primary hippocampal neuronal cultures demonstrates the important role of neuronal autophagy in regulating memory and hippocampal synaptic plasticity. Although our study focuses on hippocampal neurons, we cannot exclude the possibility that autophagy activity in other hippocampal cell populations may also contribute to the regulation of memory formation and cognitive fitness. Indeed, the pharmacological targeting of autophagy after hippocampal injections does not selectively target neuronal autophagy, and other cell populations could also partially contribute to memory formation and age-impaired memory performances. Moreover, autophagy has been shown to play a role in other cell types, such as astrocytes that prune axons [45] and oligodendrocytes that increase myelination [46]. Therefore, further analyses will be required to determine the specific hippocampal neuronal populations and possibly other cell type(s) (i.e., astrocytes), in which autophagy has a predominant effect in the control of memory formation.

Aging is commonly associated with progressive impairments in hippocampal-dependent memory [19–24] and with defective autophagy in various tissues [29–31]. We show that autophagy activity is reduced in the hippocampus during aging and that

Figure 6. Youthful Circulating Factors, Such as Osteocalcin, Improve Age-Related Memory Deficits in an Autophagy-Dependent Manner

(A) LC3-I and II abundance (representative western blot, left) and LC3-II/β-actin band intensity quantification (right) in the hippocampi of 3- or 16-month-old mice after tail vein injections with either vehicle (n = 5 or 5), plasma derived from young (8-week-old: young plasma [YP]; n = 5 or 5) or old (18-month-old: old plasma [OP]; n = 3–5) mice. β-actin was used as a loading control for each sample. These measurements were obtained from 3 independent experiments. See also Figure S6.

(B) NOR performed in 3- (n = 8) and 16-month-old mice (n = 7 or 8) 3 weeks after local hippocampal infections with either AAV-*Beclin 1*-shRNA or AAV-Scramble-shRNA and subjected to 7 tail vein injections over 24 days of either vehicle or YP (derived from 8-week-old mice). Discrimination index and preference index were measured for each group during the testing phase. The NOR was performed on one cohort of mice for each group. See also Figure S6.

(C) LC3-I and II accumulation (left) and quantification data (right; LC3-II/β-actin ratio) in mature primary hippocampal neurons treated with either NaCl, bafilomycin A1 (Baf), Ocn (10 ng/mL), or Ocn + Baf. The quantification is represented in comparison to NaCl group. These measurements were obtained from n = 3 individual hippocampal neuronal preparations.

(D) LC3-I and II accumulation 12 hr after hippocampal stereotactic injections of either vehicle or osteocalcin (Ocn) (10 ng/hemisphere) in 3- or 16-month-old mice (n = 4). This analysis was performed on two independent cohorts of mice for each group. See also Figure S6.

(E) LC3-I and II accumulation (representative western blot, left) and quantification data (LC3-II/β-actin ratio, right) in the hippocampi of 3- or 16-month-old mice after tail vein injections with vehicle (n = 6 or 6) or with either IgG (YP [IgG]; n = 6) or anti-Ocn immunodepleted (YP[-Ocn]; n = 6) young plasma (derived from 8-week-old mice). β-actin was used as a loading control for each sample. These measurements were obtained from 3 independent experiments. See also Figure S6.

(F) NOR performed in 3- (n = 8) and 16-month-old mice (n = 7–9), after hippocampal stereotactic injections of either AAV-eSYN-*Beclin 1*-shRNAmir or AAV-Scramble-shRNA and infused peripherally and continuously through minipumps with uncarboxylated Ocn (30 ng/hr) or vehicle (NaCl). Discrimination index and preference index were measured for each group during the testing phase. The NOR was performed in two independent experiments for each group of mice. See also Figure S6.

Independent cohorts of mice were used for each behavioral test (no mice were used in more than one behavioral test). All behavioral tests were performed on $n \geq 7$ mice per group. Data are expressed as mean ± SEM. *$p \leq 0.05$; **$p \leq 0.01$; ***$p \leq 0.001$; NS, not significant by Student's t test and by one-way ANOVA followed by a post hoc Tuckey's HSD multiple comparisons test for pairwise differences between each group of mice.

promoting autophagy in old hippocampi is necessary and sufficient to improve age-related hippocampal-dependent memory deficiencies. These results reinforce the link between autophagy and aging and underscore the importance of maintaining autophagy capacity in the brain for cognitive fitness throughout life. This has important clinical implications in preventing and/or treating cognitive impairments in aging populations, as autophagy is directly targetable by drugs [47], and its pharmacological induction could be amenable to significant therapeutic benefits [48, 49]. It is important to note that, during brain aging, the alterations in dendritic spines formation are subtle and region specific [4]. Consequently, the influence of autophagy on dendritic spine formation may not be directly related to its beneficial effects on age-related cognitive deficits. However, our demonstration that autophagy is required for activity-dependent dendritic spine formation may help to partially modulate mechanisms of plasticity that could be affected in various cognitive disorders. Moreover, the decrease in autophagy activity observed in old hippocampi is not restricted to neurons, but it is also present in some astrocytes, both in the CA3 and DG regions. This suggests a possible role for autophagy in astrocytes in age-impaired memory and brain aging processes.

Perhaps the most intriguing finding of our study is the demonstration that spiked systemic administrations of young plasma improve age-impaired autophagy levels in the hippocampus [25–28] and that the rejuvenating effects of young plasma injections on memory decline during aging are abrogated after the downregulation of hippocampal autophagy. These findings favor the notion that young blood factors reverse age-dependent alterations in memory by restoring autophagy levels in old hippocampi. They also suggest a prominent role for brain autophagy in mediating the communication between systemic milieu and hippocampal neurons for fostering cognitive fitness throughout life.

Although the mechanisms involved in the age-associated decline of autophagy are still being elucidated, our results suggest that the loss or decrease of young circulating factors in plasma contribute to this decline. Among these factors, Ocn, a bone-derived hormone that passes through the blood-brain barrier and influences hippocampal-dependent memory by binding to the G-coupled receptor Gpr158 in hippocampal neurons [28, 38–41], has been recently identified as a necessary component of young plasma for improving the deleterious effects of aging on learning and memory. We demonstrate here that Ocn injections in aged mice are sufficient to significantly ameliorate age-impaired autophagy in old hippocampi, requiring autophagy to mediate its beneficial effect on age-related cognitive decline. Whereas the role of autophagy as a mediator in the dialogue between peripheral organs is well described (e.g., pancreatic hormones in the regulation of liver autophagy), this study highlights for the first time a key role for autophagy in shaping the communication between peripheral tissues and the brain. The identification of Ocn as a novel hormonal inducer of autophagy does not exclude the contribution of other systemic circulating factors in fostering hippocampal memory capacities via induction of autophagy, which is also suggested by the partial rescue of hippocampal autophagy levels observed after systemic injections of young plasma immunodepleted for Ocn. However, this provides new insights into the larger role of autophagy in the mediation of hormonal actions on cognitive function.

In summary, we show here that autophagy plays a key role in promoting the formation of new memory in hippocampal neurons by modulating structural and functional activity-dependent synaptic plasticity. Impaired hippocampal autophagy activity is observed during aging and leads to memory decline, and restoring autophagy levels in old hippocampi is sufficient to reverse age-related memory deficits. Autophagy promotes the effects of systemic administrations of young plasma on brain cognitive fitness. Among these factors, we identified Ocn has a novel anti-geronic hormonal inducer of autophagy in hippocampal neurons, highlighting the role of autophagy in mediating hormonal regulation of neuronal and behavioral functions in the brain. Altogether, these findings underlie novel physiological functions for autophagy in the brain for promoting the adaptive responses of the hippocampal neurons to novel stimulations and systemic factors and may guide the development of treatments for aged-memory decline in aging populations.

STAR★METHODS

Detailed methods are provided in the online version of this paper and include the following:

- KEY RESOURCES TABLE
- CONTACT FOR REAGENT AND RESOURCE SHARING
- EXPERIMENTAL MODEL AND SUBJECT DETAILS
  - Animals
- METHOD DETAILS
  - Western blot analysis
  - SQSTM1/p62 puncta immunostaining and quantification
  - Semiquantitative RT-PCR
  - Stereotaxic surgery
  - Pharmacological modulation of autophagy
  - Adeno-associated viruses expressing shRNA
  - Behavioral tests
  - Memory-related stimulation procedures
  - Restraint procedure
  - Plasma collection and intravenously injection
  - Immunodepletion of Ocn from plasma
  - Recombinant Ocn
  - Osmotic pumps
  - Primary cultured hippocampal neurons
  - Neuronal stimulation treatment of primary hippocampal neurons
  - Lentiviral infections and transfection of primary hippocampal neurons
  - Dendritic spines density analysis *in vitro*
  - Golgi Cox Staining and dendritic spines quantification
  - TUNEL Assay
  - Electrophysiology
- QUANTIFICATION AND STATISTICAL ANALYSIS
- DATA AND SOFTWARE AVAILABILITY
  - Data resources

SUPPLEMENTAL INFORMATION

Supplemental Information includes six figures and can be found with this article online at https://doi.org/10.1016/j.cub.2018.12.021.

ACKNOWLEDGMENTS

We thank Drs. S. Lotersztajn, A. Chamouni, A.N. Armand, and G. Karsenty for critical reading of the manuscript and suggestions during the course of the study. We thank the lentiviral core and animal house facility of the SFR Necker. This work was supported by the Fondation pour la Recherche Médicale (FRM-AJE20130928594; F.O. and M.R.B.), Human Frontier Scientific Program (HFSP) (F.O.), ATIP-AVENIR Program (F.O.), NARSAD Young Investigator Award (A.K.F.), AGEMED-INSERM Program (F.O. and P.C.), ANR (F.O., P.C., and G.F.), and the Fondation Schlumberger pour l'Education et la Recherche (FSER) (F.O.).

AUTHOR CONTRIBUTIONS

A.K.F., E.M., C.S., A.B., P.C., and F.O. designed the experiments; M.G., S.M., M.R., F.L., and M.R.-B. performed all of the experiments with help from N.B.; A.R. performed for *in vitro* and *in vivo* neuronal plasticity analyses; and A.C.N. performed histological analyses. M.R.S. performed all of the electrophysiological experiments; M.G., S.M., M.R., M.R.-B., A.K.F., F.L., A.B., P.C., E.M., and F.O. analyzed and interpreted the data; and S.M., G.F., F.L., A.B., N.K., P.C., and F.O. wrote the manuscript.

DECLARATION OF INTERESTS

The authors declare no competing interests.

Received: April 2, 2018
Revised: September 25, 2018
Accepted: December 13, 2018
Published: January 17, 2019

REFERENCES

1. Bishop, N.A., Lu, T., and Yankner, B.A. (2010). Neural mechanisms of ageing and cognitive decline. Nature *464*, 529–535.
2. Leuner, B., and Gould, E. (2010). Structural plasticity and hippocampal function. Annu. Rev. Psychol. *61*, 111–140, C1–C3.
3. Bailey, C.H., and Kandel, E.R. (1993). Structural changes accompanying memory storage. Annu. Rev. Physiol. *55*, 397–426.
4. Bartsch, T., and Wulff, P. (2015). The hippocampus in aging and disease: From plasticity to vulnerability. Neuroscience *309*, 1–16.
5. Wang, Y.C., Lauwers, E., and Verstreken, P. (2017). Presynaptic protein homeostasis and neuronal function. Curr. Opin. Genet. Dev. *44*, 38–46.
6. Kulkarni, A., Chen, J., and Maday, S. (2018). Neuronal autophagy and intercellular regulation of homeostasis in the brain. Curr. Opin. Neurobiol. *51*, 29–36.
7. Vijayan, V., and Verstreken, P. (2017). Autophagy in the presynaptic compartment in health and disease. J. Cell Biol. *216*, 1895–1906.
8. Kulkarni, V.V., and Maday, S. (2018). Compartment-specific dynamics and functions of autophagy in neurons. Dev. Neurobiol. *78*, 298–310.
9. Shen, W., and Ganetzky, B. (2009). Autophagy promotes synapse development in Drosophila. J. Cell Biol. *187*, 71–79.
10. Shehata, M., Matsumura, H., Okubo-Suzuki, R., Ohkawa, N., and Inokuchi, K. (2012). Neuronal stimulation induces autophagy in hippocampal neurons that is involved in AMPA receptor degradation after chemical long-term depression. J. Neurosci. *32*, 10413–10422.
11. Mizushima, N., and Komatsu, M. (2011). Autophagy: renovation of cells and tissues. Cell *147*, 728–741.
12. Boya, P., Reggiori, F., and Codogno, P. (2013). Emerging regulation and functions of autophagy. Nat. Cell Biol. *15*, 713–720.
13. Mizushima, N., Yoshimori, T., and Ohsumi, Y. (2011). The role of Atg proteins in autophagosome formation. Annu. Rev. Cell Dev. Biol. *27*, 107–132.
14. Lamb, C.A., Yoshimori, T., and Tooze, S.A. (2013). The autophagosome: origins unknown, biogenesis complex. Nat. Rev. Mol. Cell Biol. *14*, 759–774.
15. Ktistakis, N.T., and Tooze, S.A. (2016). Digesting the expanding mechanisms of autophagy. Trends Cell Biol. *26*, 624–635.
16. Galluzzi, L., Pietrocola, F., Levine, B., and Kroemer, G. (2014). Metabolic control of autophagy. Cell *159*, 1263–1276.
17. Singh, R., and Cuervo, A.M. (2011). Autophagy in the cellular energetic balance. Cell Metab. *13*, 495–504.
18. Nixon, R.A. (2013). The role of autophagy in neurodegenerative disease. Nat. Med. *19*, 983–997.
19. Mattson, M.P., and Magnus, T. (2006). Ageing and neuronal vulnerability. Nat. Rev. Neurosci. *7*, 278–294.
20. Gray, D.T., and Barnes, C.A. (2015). Distinguishing adaptive plasticity from vulnerability in the aging hippocampus. Neuroscience *309*, 17–28.
21. Grady, C. (2012). The cognitive neuroscience of ageing. Nat. Rev. Neurosci. *13*, 491–505.
22. Burke, S.N., and Barnes, C.A. (2010). Senescent synapses and hippocampal circuit dynamics. Trends Neurosci. *33*, 153–161.
23. Harada, C.N., Natelson Love, M.C., and Triebel, K.L. (2013). Normal cognitive aging. Clin. Geriatr. Med. *29*, 737–752.
24. Hedden, T., and Gabrieli, J.D. (2004). Insights into the ageing mind: a view from cognitive neuroscience. Nat. Rev. Neurosci. *5*, 87–96.
25. Villeda, S.A., Luo, J., Mosher, K.I., Zou, B., Britschgi, M., Bieri, G., Stan, T.M., Fainberg, N., Ding, Z., Eggel, A., et al. (2011). The ageing systemic milieu negatively regulates neurogenesis and cognitive function. Nature *477*, 90–94.
26. Villeda, S.A., Plambeck, K.E., Middeldorp, J., Castellano, J.M., Mosher, K.I., Luo, J., Smith, L.K., Bieri, G., Lin, K., Berdnik, D., et al. (2014). Young blood reverses age-related impairments in cognitive function and synaptic plasticity in mice. Nat. Med. *20*, 659–663.
27. Castellano, J.M., Mosher, K.I., Abbey, R.J., McBride, A.A., James, M.L., Berdnik, D., Shen, J.C., Zou, B., Xie, X.S., Tingle, M., et al. (2017). Human umbilical cord plasma proteins revitalize hippocampal function in aged mice. Nature *544*, 488–492.
28. Khrimian, L., Obri, A., Ramos-Brossier, M., Rousseaud, A., Moriceau, S., Nicot, A.S., Mera, P., Kosmidis, S., Karnavas, T., Saudou, F., et al. (2017). Gpr158 mediates osteocalcin's regulation of cognition. J. Exp. Med. *214*, 2859–2873.
29. Rubinsztein, D.C., Mariño, G., and Kroemer, G. (2011). Autophagy and aging. Cell *146*, 682–695.
30. Cuervo, A.M. (2008). Autophagy and aging: keeping that old broom working. Trends Genet. *24*, 604–612.
31. Shibata, M., Lu, T., Furuya, T., Degterev, A., Mizushima, N., Yoshimori, T., MacDonald, M., Yankner, B., and Yuan, J. (2006). Regulation of intracellular accumulation of mutant Huntingtin by Beclin 1. J. Biol. Chem. *281*, 14474–14485.
32. Fioriti, L., Myers, C., Huang, Y.Y., Li, X., Stephan, J.S., Trifilieff, P., Colnaghi, L., Kosmidis, S., Drisaldi, B., Pavlopoulos, E., and Kandel, E.R. (2015). The persistence of hippocampal-based memory requires protein synthesis mediated by the prion-like protein CPEB3. Neuron *86*, 1433–1448.
33. Shoji-Kawata, S., Sumpter, R., Leveno, M., Campbell, G.R., Zou, Z., Kinch, L., Wilkins, A.D., Sun, Q., Pallauf, K., MacDuff, D., et al. (2013). Identification of a candidate therapeutic autophagy-inducing peptide. Nature *494*, 201–206.
34. Derkach, V.A., Oh, M.C., Guire, E.S., and Soderling, T.R. (2007). Regulatory mechanisms of AMPA receptors in synaptic plasticity. Nat. Rev. Neurosci. *8*, 101–113.
35. Bliss, T.V., and Collingridge, G.L. (1993). A synaptic model of memory: long-term potentiation in the hippocampus. Nature *361*, 31–39.
36. Jiang, X., Chai, G.S., Wang, Z.H., Hu, Y., Li, X.G., Ma, Z.W., Wang, Q., Wang, J.Z., and Liu, G.P. (2015). Spatial training preserves associative memory capacity with augmentation of dendrite ramification and spine generation in Tg2576 mice. Sci. Rep. *5*, 9488.

37. Mahmmoud, R.R., Sase, S., Aher, Y.D., Sase, A., Gröger, M., Mokhtar, M., Höger, H., and Lubec, G. (2015). Spatial and working memory is linked to spine density and mushroom spines. PLoS ONE *10*, e0139739.
38. Kosmidis, S., Polyzos, A., Harvey, L., Youssef, M., Denny, C.A., Dranovsky, A., and Kandel, E.R. (2018). RbAp48 Protein is a critical component of GPR158/OCN signaling and ameliorates age-related memory loss. Cell Rep. *25*, 959–973.e6.
39. Oury, F., Khrimian, L., Denny, C.A., Gardin, A., Chamouni, A., Goeden, N., Huang, Y.Y., Lee, H., Srinivas, P., Gao, X.B., et al. (2013). Maternal and offspring pools of osteocalcin influence brain development and functions. Cell *155*, 228–241.
40. Khrimian, L., Obri, A., and Karsenty, G. (2017). Modulation of cognition and anxiety-like behavior by bone remodeling. Mol. Metab. *6*, 1610–1615.
41. Obri, A., Khrimian, L., Karsenty, G., and Oury, F. (2018). Osteocalcin in the brain: from embryonic development to age-related decline in cognition. Nat. Rev. Endocrinol. *14*, 174–182.
42. Mera, P., Laue, K., Wei, J., Berger, J.M., and Karsenty, G. (2016). Osteocalcin is necessary and sufficient to maintain muscle mass in older mice. Mol. Metab. *5*, 1042–1047.
43. Hernandez, D., Torres, C.A., Setlik, W., Cebrián, C., Mosharov, E.V., Tang, G., Cheng, H.C., Kholodilov, N., Yarygina, O., Burke, R.E., et al. (2012). Regulation of presynaptic neurotransmission by macroautophagy. Neuron *74*, 277–284.
44. Liang, Y., and Sigrist, S. (2018). Autophagy and proteostasis in the control of synapse aging and disease. Curr. Opin. Neurobiol. *48*, 113–121.
45. Song, J.W., Misgeld, T., Kang, H., Knecht, S., Lu, J., Cao, Y., Cotman, S.L., Bishop, D.L., and Lichtman, J.W. (2008). Lysosomal activity associated with developmental axon pruning. J. Neurosci. *28*, 8993–9001.
46. Smith, C.M., Mayer, J.A., and Duncan, I.D. (2013). Autophagy promotes oligodendrocyte survival and function following dysmyelination in a long-lived myelin mutant. J. Neurosci. *33*, 8088–8100.
47. Madeo, F., Tavernarakis, N., and Kroemer, G. (2010). Can autophagy promote longevity? Nat. Cell Biol. *12*, 842–846.
48. De Stefano, D., Villella, V.R., Esposito, S., Tosco, A., Sepe, A., De Gregorio, F., Salvadori, L., Grassia, R., Leone, C.A., De Rosa, G., et al. (2014). Restoration of CFTR function in patients with cystic fibrosis carrying the F508del-CFTR mutation. Autophagy *10*, 2053–2074.
49. Rubinsztein, D.C., Codogno, P., and Levine, B. (2012). Autophagy modulation as a potential therapeutic target for diverse diseases. Nat. Rev. Drug Discov. *11*, 709–730.
50. Schneider, C.A., Rasband, W.S., and Eliceiri, K.W. (2012). NIH Image to ImageJ: 25 years of image analysis. Nat. Methods *9*, 671–675.
51. Oh, M.C., and Derkach, V.A. (2005). Dominant role of the GluR2 subunit in regulation of AMPA receptors by CaMKII. Nat. Neurosci. *8*, 853–854.

STAR★METHODS

KEY RESOURCES TABLE

REAGENT or RESOURCE	SOURCE	IDENTIFIER
Antibodies		
Mouse anti-β-actin (1/5000)	Sigma	CAT# 2228; RRID:AB_476697
Mouse anti-Beclin 1 (1:1000)	BD Transduction Laboratories	CAT# 612113; RRID:AB_399484
Rabbit anti-LC3 (1:10000)	Sigma-Aldrich	CAT# L7543; RRID:AB_796155
Mouse anti-ATG5 (1:500)	Nanotools	CAT# 0262-100; ATG5-7C6
Rabbit anti-VPS34 (1:1000)	Cell Signaling	CAT# 4263; RRID:AB_2299765
Mouse anti-GFAP (1:400)	abcam	CAT# ab10062; RRID:AB_296804
Mouse anti-NeuN (1:500)	Millipore	CAT# MAB377; RRID:AB_2298767
Anti-mouse IgG, HRP-linked antibody (1: 5000)	Cell Signaling	CAT# 7076; RRID:AB_330924
Guinea pig anti-p62 (1:2000)	Progen	CAT# GP62C; RRID:AB_2687531
Anti-rabbit IgG, HRP-linked antibody (1: 5000)	Cell Signaling	CAT# 7074; RRID:AB_2099233
Anti- Guinea pig IgG, HRP-linked antibody (1:25000)	Sigma-Aldrich	CAT# A5545; RRID:AB_258247
Donkey anti-guinea pig IgG Alexa Fluor 488 (1:200)	Bioss	CAT# bs-0358D-A488; RRID:AB_10891275
Donkey anti-Mouse IgG (H+L) Highly Cross-Adsorbed Secondary Antibody, Alexa Fluor 546 (1:800)	Thermo Fisher Scientific	Cat# A10036; RRID:AB_2534012
Anti-C-terminal OCN antibody	[18]	N/A
Goat IgG Control	R&Dsystems	CAT# AB-108 C; RRID:AB_354267
Bacterial and Virus Strains		
AAV9-GFP-U6-mBECN1-shRNA (*Becn 1*)	Vector Biosystems (Malvern PA)	CAT# shAAV-253929
AAV9-GFP-U6-M-RB1CC1-shRNA (*Fip200*)	Vector Biosystems (Malvern PA)	CAT# shAAV-270212
AAV9-GFP-U6-m-ATG12-shRNA (*Atg12*)	Vector Biosystems (Malvern PA)	CAT# shAAV-253216
AAV-GFP-U6-scrmb-shRNA	Vector Biosystems (Malvern PA)	CAT#7045
AAV9-eSYN-GFP-Beclin 1-shRNAmir	Vector Biosystems (Malvern PA)	Build-to-Order
AAV-*eSYN-GFP*-shRNA155mir	Vector Biosystems (Malvern PA)	Build-to-Order
Lentiviruses (pLKO-IPTG-3XLacO) expressing an IPTG (Isopropyl β-D-1-thiogalactopyranoside)-inducible shRNA targeting mouse Beclin-1 (*Becn 1*)	Sigma-Aldrich	CAT#SHC332
Biological Samples		
Mouse uncarboxylated Ocn	[39] (Provided by Dr. Gerard Karsenty – Columbia University-Medical Center, New york, USA)	N/A
Young plasma immunodepleted for Ocn	[18] (Provided by Dr. Gerard Karsenty – Columbia University-Medical Center, New york, USA)	N/A
Young plasma treated with IgG	[18] (Provided by Dr. Gerard Karsenty – Columbia University-Medical Center, New york, USA)	N/A
Chemicals, Peptides, and Recombinant Proteins		
Tat–Beclin 1 (YGRKKRRQRRRGG TNVFNATFEIWHDGEFGT)	[33] (Provided by Dr. Carmine Settembre - TIGEM, Naples, Italy)	N/A
TAT-Scramble (YGRKKRRQRRRGGV GNDFFINHETTGFATEW)	[33] (Provided by Dr. Carmine Settembre - TIGEM, Naples, Italy)	N/A

(*Continued on next page*)

Continued

REAGENT or RESOURCE	SOURCE	IDENTIFIER
Spautin-1	Sigma-Aldrich	CAT#SML0440
Leupeptin	Sigma-Aldrich	CAT#L2023
Chloroquine	Sigma-Aldrich	CAT#C6628
Bafilomycin A1	Sigma-Aldrich	CAT# B1793-10UG
Critical Commercial Assays		
TUNNEL assay (ApopTag® Peroxidase *In Situ* Apoptosis)	Millipore	CAT#S7100
FD Rapid GolgiStain Kit	FD Neuro Technologies, Baltimore, MD	CAT# PK401
Experimental Models: Cell Lines		
Primary Hippocampal neurons (fresh preparation)	This paper	N/A
Experimental Models: Organisms/Strains		
C57BL/6J WT male mice (3 and 16 month-old)	Janvier Laboratory-Le Genest St Isle, France	CAT# SC-C57J-M
Swiss WT male mice (3 month-old)	Janvier Laboratory-Le Genest St Isle, France	CAT# RjOrl:SWISS
Oligonucleotides		
Becn 1 primer Forward: 5′-ATGGAG GGGTCTAAGGCGTC-3′	This paper	N/A
Becn 1 primer Reverse: 5′-TCCTCT CCTGAGTTAGCCTCT-3′	This paper	N/A
Vps34 primer Forward: 5′- CCTGGA CATCAACGTGCAG-3′	This paper	N/A
Vps34 primer Reverse: 5′-TGTCTC TTGGTATAGCCCAGAAA-3′	This paper	N/A
Atg5 primer Forward: 5′-TGTGCT TCGAGATGTGTGGTT-3′	This paper	N/A
Atg5 primer Reverse: 5′-GTCAAAT AGCTGACTCTTGGCAA-3′		N/A
GAPDH primers Forward: 5′-AACAT CCATCGCGGTCTC-3′	This paper	N/A
GAPDH primers Reverse: 5′-CCATT TTGTCTACGGGACGA-3′	This paper	N/A
Software and Algorithms		
GraphPad Prism 5.0.	GraphPad	RRID:SCR_002798
Packwin 2.0 software	Bioseb (France)	https://www.panlab.com/en/products/packwin-software-panlab
ActiMot2 Software	(PhenoMaster Software, TSE System, Germany)	https://www.tse-systems.com/product-details/phenomaster/actimot?open=1228
Icy Software	Icy	RRID:SCR_010587
NeuronStudio softare	NeuronStudio	RRID:SCR_013798
NeuronJ software	NeuronJ	RRID:SCR_002074
ImageJ 1.x	[50]	PMID 22930834
Image Lab software (Version 5.2)	BioRad	http://www.bio-rad.com/fr-fr/product/image-lab-software?ID=KRE6P5E8Z
Other		
Alzet micro-osmotic pumps (model 1002)	Alzet	ALZT1002

CONTACT FOR REAGENT AND RESOURCE SHARING

Further information and requests for resources and reagents should be directed to and will be fulfilled by the Lead Contact, Franck Oury (franck.oury@inserm.fr).

EXPERIMENTAL MODEL AND SUBJECT DETAILS

Animals

All experiments were performed on C57BL/6J WT male mice (obtained from Janvier Laboratory, Le Genest St Isle, France). All mice were 3 or 16 months of age at the start of experiments. For all experiments, we used littermates as controls. Upon arrival, mice were housed at least 2 weeks before any behavioral or molecular testing. Mice were housed 5 animals per cage in polycarbonate cages (35.5 × 18 × 12.5 cm), under a 12 hours light/dark cycle with *ad libitum* access to food and water prior to experimentation. All behavioral experiments were performed between 10AM and 5PM. In all experiments, animals were randomly assigned to treatment groups. Group sizes were determined after performing a power calculation to lead to an 80% chance of detecting a significant difference ($p \leq 0.05$). All behavioral experiments were performed in accordance with the European Communities for Experimental animal use (2010/63/EU) and local ethical committee review procedures and protocols (APAFIS - 13939 - 201803071644868v1).

METHOD DETAILS

Western blot analysis

Mouse dorsal hippocampi and cerebellum were dissected, snap frozen and lysed in RIPA lysis buffer (25mM Tris HCl, pH 7.6, 150mM NaCl, 1% NP40, 1% Na deoxycholate, 0.1% SDS and cOmplete protease and phosphatase inhibitors). The lysates were loaded on a 12% SDS polyacrylamide gradient gel and transferred onto a PVDF membrane. The blots were blocked in Tris-buffered saline with Tween (TBST)-5% BSA and incubated with either mouse anti-β-actin (1:5000, A-2228: Sigma), mouse anti-Beclin 1 (1:1000, 612113: BD Transduction Laboratories, only the top band corresponding to non-cleaved Beclin 1 was quantified in this study), rabbit anti-LC3 (1:10000, L7543: Sigma), mouse anti-ATG5 (1:500, 0262-100/ATG5-7C6: Nanotools), rabbit anti-VPS34 (1:1000; 4263: Cell Signaling), and guinea pig anti-p62 (1:2000, GP62-C: Progen). Horseradish peroxidase–conjugated secondary antibodies (anti-mouse IgG, HRP-linked antibody (7076, Cell Signaling) and anti-rabbit IgG, HRP-linked antibody (7074: Cell Signaling) and anti-guinea pig IgG, HRP-linked antibody (A5545: sigma) revealed using an ECL kit (Clarity Western ECL Substrate: BioRad) for protein detection. Selected films were scanned and quantified using BioRad Image Lab software (Version 5.2). β-actin bands were used for normalization. All Western-blot analyses were performed on freshly prepared hippocampal or cerebellum lysates.

SQSTM1/p62 puncta immunostaining and quantification

Mice were deeply anesthetized with a mixture Ketamine/Xylazine and transcardially perfused with cold PBS, followed by cold 4% PFA. Brains were post-fixed overnight in 4%PFA at 4°C. 30 μm serial coronal floating sections were obtained using a vibratome. For the single immunofluorescence, sections were blocked with 10% fetal bovine serum for 30 min at room temperature and then incubated with guinea pig anti-p62 (1:200, GP62C: Progen) overnight at 4°C. The sections were washed with PBS before and after being incubated with an Alexa Fluor-conjugated secondary antibody (donkey anti-guinea pig IgG (1:200, Alexa Fluor 488: Bioss inc.) for 1 hour at room temperature in blocking buffer. For the co-immunofluorescences, we used guinea pig anti-p62 (1:200, GP62C: Progen) with either mouse anti-NeuN (1:500, Millipore) or mouse anti-GFAP (1:400, Abcam). The sections were washed with PBS before and after being incubated with an Alexa Fluor-conjugated secondary antibodies (donkey anti-guinea pig IgG (1:200, Alexa Fluor 488: Bioss inc.; and donkey anti-mouse IgG (1:800, Alexa Fluor 546: Bioss inc.) for 2h at room temperature in blocking buffer. All sections were mounted onto gelatin-subbed slides and coverslipped using Mowiol with DAPI. Images were obtained using a Zeiss Apotome2 fluorescence microscope and analyzed using Zen light Zeiss LSM software. The number of cells with SQSTM1/p62 puncta was quantified on digital images with Icy software (http://icy.bioimageanalysis.org).

Semiquantitative RT-PCR

Brain tissues were immediately flash-frozen after dissection and total RNA was isolated with TRIzol Reagent using a homogenizer. Single-strand cDNA was synthesized from total RNA (2 μg) by using SuperScript II Reverse Transcriptase. qRT–PCR was performed using iTAQ SYBR Green (BioRad). The following primers were used: *Becn 1* primers (5′-ATGGAGGGGTCTAAGGCGTC-3′ and 5′-TCCTCTCCTGAGTTAGCCTCT-3′), *Atg5* primers (5′-TGTGCTTCGAGATGTGTGGTT-3′ and 5′-GTCAAATAGCTGACTCTTGG CAA-3′), *Vps34* primers (5′-CCTGGACATCAACGT GCAG-3′ and 5′-TGTCTCTTGGTATAGCCCAGAAA-3′), *FIP200* primers (5′-GAC ACTG AGCTAACTGTGCAA-3′ and 5′-GCGCTGTAAGTACACACTCTT C-3′), and *ATG12* primers (5′-TTCGGTTGCAGT TTCGC C-3′ and 5′-CCATGCCTGTGATTTGCAGTA-3′).

Stereotaxic surgery

Mice were anesthetized by intraperitoneal injection of ketamine hydrochloride (20mg/ml BW) (1000 Virbac) and xylazine (100mg/ml BW) (Rompun 2%; Bayer) and placed in a stereotaxic frame (900SL-KOPF). Ophthalmic eye ointment was applied to the cornea to prevent desiccation during surgery. The area around the incision was trimmed and Vétoquinol was applied. All drugs were injected bilaterally into the dorsal hippocampi using the following coordinates (from Bregma, Paxinos and Franklin, 2008): X = +/−1.4 mm, Y = 2.0 mm and Z = −1.33 mm. A 1 μL volume of either AAV or drugs was injected stereotaxically over 4 min (injection rate: 0.25 μL per min). To limit reflux along the injection track, the needle was maintained *in situ* for 4 min between each 1 μL injection.

Pharmacological modulation of autophagy

For pharmacological hippocampal induction of autophagy, we performed intra-hippocampal injections of either vehicle (PBS), 1 μg TAT-Scramble (dissolved in PBS) or 1 μg TAT-Beclin 1 (dissolved in PBS). The Tat-Beclin 1 (YGRKKRRQRRRGGTNVFNAT FEIWHDGEFGT) consisted of 11 amino acids of the TAT protein transduction domain (PTD) at the N terminus, a GG linker to increase flexibility, and 18 amino acids derived from Beclin 1, amino acids 267–284 containing 3 substitutions: H275E, S279D, Q281E. Control peptide, TAT-Scramble (YGRKKRRQRRRGGV GNDFFINHETTGFATEW), consisted of the TAT protein transduction domain, a GG linker, and a scrambled version of the C-terminal 18 amino acids from Tat-Beclin 1. For pharmacological hippocampal inhibition of autophagy formation, we performed intra-hippocampal injections of either Spautin-1 (5 μg (SML0440: Sigma) dissolved in DMSO/NaCl) or vehicle (DMSO/NaCl). For pharmacological hippocampal inhibition of the late stage of the autophagic pathway, we performed stereotactic injections of either 100ng Leupeptin (L2023: Sigma) (dissolved in PBS), 50 μg Chloroquine (C6628: Sigma) (dissolved in PBS) or vehicle (PBS). All drugs were infused in a volume of 1 μL (bilaterally) in the dorsal hippocampus either 12 hours before training phase or 12 hours before the testing phase for the NOR, CFC or OLM behavioral tasks. For brain collection hippocampal stereotactic injections were performed either 12 or 36 hours before sacrifice.

Adeno-associated viruses expressing shRNA

Adeno-associated viruses (AAV) expressing shRNA were purchased from Vector Biosystems Inc (Malvern PA). shRNAs specific to Beclin 1 (*Becn 1*) (AAV9-GFP-U6-mBECN1-shRNA), FiP200 (AAV9-GFP-U6-M-RB1CC1-shRNA), ATG12 (AAV9-GFP-U6-m-ATG12-shRNA) or scrambled non-targeting negative control (AAV-GFP-U6-scrmb-shRNA) were injected in a volume of 1 μL (bilaterally), 3 weeks prior to behavioral tests or brain tissue collection. The AAV titers were between 2.8 and 4.3 × 10^{13} GC/ml. AAV expressing shRNAmir targeting Beclin 1 (*Becn 1*) specifically in neurons (AAV9-eSYN-GFP-Beclin 1-shRNAmir) were purchased from Vector Biosystems Inc (Malvern PA). Beclin 1 shRNAmir is driven by the eSYN promoter, a hybrid promoter consisting of the 0,45Kb human Synapsin 1 promoter fragment (hSYN1). AAV-*eSYN-GFP*-shRNA155mir was used as control. The AAV titers were between 5.3 and 5.9 × 10^{13} GC/ml.

Behavioral tests

Novel object recognition paradigm (NOR)

The behavior sessions were recorded with a video camera. The testing arena consisted on two plastic boxes (60 × 40 × 32 cm). Mice could not contact or see each other during the exposures. The light intensity was equal in all parts of the arena. Two different objects were used, available in triplicate: (A) a blue ceramic pot (diameter 6.5 cm, maximal height 7.5 cm) and (B) a clear/plastic funnel (diameter 8.5 cm, maximal height 8.5 cm). The objects elicited equal levels of exploration as determined in pilot experiments and training phase. Mice were transported a short distance from the holding mouse facility to the testing room in their home cages and left undisturbed for at least two hours before the beginning of the test. Mice were always placed in the center of the arena at the start of each exposure.

The NOR paradigm consists of three phases over 3 days. On day 1 (habituation phase): mice were given 5 min to explore the arena, without any objects and were then taken back to their home cage or for stereotactic surgery. On day 2 (training phase): mice were allowed to explore, for 10 min, two identical objects arranged in a symmetric opposite position from the center of the arena and were then transported to their home cage. On day 3 (testing phase): mice were given 15 minutes to explore two objects: a familiar object and a novel one, in the same arena, keeping the same object localization. The object that serves as a novel object (A or B), as well as the left/right localization of the objects were counterbalanced within each group. Between exposures, arenas were cleaned with phagosphore, and the bedding replaced. The following behaviors were considered as exploration of the objects: sniffing or touching the object with the nose or with the front legs or directing the nose to the object at a distance $\leq$ 1 cm. Investigation was not scored if the mouse was on top of the object or completely immobile. The preference index (time spent exploring the new object / the total time spent exploring both objects) and the discrimination index (time spent exploring the new object - time spent exploring the familiar object) / (total time spent exploring both objects) were calculated. As control, preference index for the (right versus left) object location or for the object A versus B during the training phase of the NOR was measured in all groups of mice exposed to the test. Behavior was scored on videos by two observers blind to treatment and the total exploration time of the objects was quantified during the training and testing phases.

Object location memory test (OLM)

For the object location memory task, all procedures were identical to the NOR except that during the testing phase, rather than presenting a novel object, mice encountered both familiar objects, with one object located in a different place in the arena. The time and frequency of exploration of the novel/relocated object is measured as an index of memory. Behavior was scored on videos by two observers blind to treatment and the total exploration time of the objects was quantified in the training and testing phases.

3-foot shock contextual fear conditioning (CFC)

Mice were left undisturbed for at least two hours before the beginning of the test. The conditioning chambers were obtained from Bioseb (France). Each chamber was located inside a larger, insulated plastic cabinet that provided protection from outside light and noise (67 × 55 × 50 cm, Bioseb, France), and mice were tested individually in the conditioning boxes. Floors of the chamber consisted of 27 stainless steel bars wired to a shock generator with scrambler for the delivery of foot shock. Signal generated by

the mice movements was recorded and analyzed through a high sensitivity weight transducer system. The analog signal was transmitted to the Freezing software module through the load cell unit for recording purposes and analysis of time active / time immobile (Freezing) was performed.

The CFC procedure took place over two consecutive days. On day 1 (training): mice were placed in the conditioning chamber, and received 3 foot-shocks (1 s, 0.5 mA), which were administrated at 60, 120 and 180 s after the animals were placed in the chamber. On day 2 (testing): contextual fear memory was assessed 24 hours after training by returning the mice to the conditioning chamber and measuring freezing behavior during a 4 min retention test. Freezing behavior was considered to occur if the animals froze for a period of at least two seconds. Freezing was scored and analyzed automatically using Packwin 2.0 software (Bioseb, France) and analyzed by two observers blind to mouse treatment or AAV-infections.

Morris Water Maze (MWM)

Animals were transported a short distance from the holding mouse facility to the testing room in their home cages and left undisturbed for at least one hour prior the first trial. Morris water maze (MWM) with an automatic tracking system was employed for assessing spatial learning and memory. The apparatus was a white circular swimming pool (diameter: 200 cm, walls: 60 cm high), which was located in a room with various distal cues. The pool was filled with water (depth: 50 cm) maintained at 22°C ± 1°C, which was made opaque by the addition of a nontoxic white paint. A 12 cm round platform was hidden 1.0 cm below the water surface. The maze was virtually divided into four arbitrary, equally spaced quadrants delineated by the cardinal points north (N), east (E), south (S), and west (W). The pool was located in a brightly lit room. Extra maze geometric and high-contrast cues were mounted on the walls of the swimming pool with the ceiling providing illumination. Each daily trial consisted of four swimming trials, in which each mouse was placed in the pool facing the wall of the tank and allowing the animal to swim to the platform before 120 s had elapsed. A trial terminated when the animal reached the platform, where it remained for 5 s. Mice were removed and placed back in their home cages for a 5 min inter-trial interval. To prevent hypothermia, the animals were gently dried with a paper towel between and after the trials. The starting point differed at each trial, and different sequences of release points were used from day to day. Animal movements were recorded using ANY-maze (Stoelting Co.) to calculate parameters of the performance of mice.

Open Field Tests (OFT)

Mice were transported a short distance from the holding facility to the testing room in their home cages and left there undisturbed for at least two hours. Each animal was placed in a 43 × 43 cm open field chamber, and tested for 30 min. Mice were placed individually into the center of the open-field arena and allowed to explore freely. Mice were monitored throughout each test session by infrared light beam activity monitor using actiMot2 Software (PhenoMaster Software, TSE System, Germany). The overall motor activity was quantified as the total distance traveled. Anxiety was also quantified by measuring the percentage of the time and distance spent in the center versus periphery of the open-field chamber.

Rotarod test

Motor function and motor learning was evaluated using an accelerating rotarod (Rota-rod/RS, Bioseb, France). On day one, mice received 2 habituation trials of 120 s (acceleration of from 4 to 20 rpm in 120 s) followed by 3 training trials of 5 min (acceleration of from 4 to 30 rpm in 5 min). On day 2, mice received 5 additional training trials. The maximum time reached in each trial was the dependent measure.

Memory-related stimulation procedures

Animals were either exposed to CFC or MWM to induce memory-related stimulations adapted from [21, 25]. For the CFC, we used one- or four-days for the training phase. For the one-day training, mice were placed into the conditioning chamber, received three shocks at 60, 120 and 180 s (1 s, 0.5 mA), and were removed 60 s following the last shock and returned to their home cages. For the four-day training, this procedure was repeated four times but at a shock intensity of 0.3 mA. Contextual fear memory was assessed 24 hours following training by returning the mice to the same conditioning chamber and measuring the freezing behavior during a 4 min retention test. For the MWM, the mice were subjected to the normal procedure (described above) for 1 day or 5 successive days. On the last day of stimulation, the mice were sacrificed 1 hour after the last exposition to CFC or MWM task.

Restraint procedure

The restraint stress group was immobilized for 30 min by a restrainer that was made of transparent acrylic, forming a cylinder (cylinder diameter of 33 mm × height of 115 mm), which restricted their movement completely. The mice were then euthanized 1 hour after the restraint stress (as we did after exposing mice to MWM or CFC). The control group was handled as the exposed group but sacrificed without restraint treatment. Then, mouse hippocampi were dissected, snap frozen and lysed in RIPA lysis buffer to perform western blot analysis to evaluate Beclin 1, p62, LC3-I and -II abundances.

Plasma collection and intravenously injection

Pooled mouse blood was collected from 80 young (8-week-old) and 20 aged (16-month-old) mice by intra-cardial bleed at the time of euthanasia. Plasma was prepared from blood collected with EDTA into Capiject T-MQK tubes followed by centrifugation at 1,000*g*. All plasma aliquots were stored at −80°C until use. Before administration, plasma was dialyzed using 3.5-kDa Maxi D-tube dialyzers (71508-3, Novagen) in PBS to remove EDTA. 16-month-old mice were injected with young, old or Ocn-immunodepleted isolated

plasma (100 μL per injection), by tail vein injection seven times over 24 days. Mice were then subjected to NOR, one day after the last injection.

Immunodepletion of Ocn from plasma

Dr. Karsenty group graciously provided us young plasma immunodepleted for Ocn (90% decrease in Ocn content) and young plasma control obtained as described in [28]. Briefly, to remove Ocn from plasma derived from 6–12-wk-old mice, anti-C-terminal Ocn antibody or goat control IgG (AB_354267: R&D Systems) was conjugated to 2.8-μm superparamagnetic M-270 Epoxy Dynabeads according to the manufacturer's instructions (Thermo Fisher Scientific), with a coupling ratio of 7 μg of antibody per 1 mg of beads. Covalent conjugation was done at 37°C for 24 h with end-over-end rotation. Coupled beads were washed with PBS before incubation with plasma to prevent detergent contamination. Plasma pooled from 6–12-wk-old C57BL/6J mice was incubated with beads coupled either to anti-C-terminal Ocn antibody or goat control IgG at 4°C overnight with end-over-end rotation, after which the plasma was dialyzed, aliquoted, and kept frozen at −80°C until use. An aliquot of plasma treated with either anti-C-terminal Ocn antibody or goat control IgG was analyzed using an Ocn ELISA to confirm significant reduction of Ocn in the immunodepleted plasma.

Recombinant Ocn

Mouse uncarboxylated Ocn was purified from BL21 bacteria transformed with pGEX2TK-mOcn as previously described [28, 38]. In brief, GST-Ocn fusion protein was bacterially produced in BL21 pLyS transformed with pGEX- 2TK-mOcn after induction with IPTG. Cells were collected in lysis buffer (PBS 1X 10 mM Tris, pH 7.2, 2 mM EDTA, 1% Triton, and 1X protease and phosphatase inhibitor cocktail; 78443; Thermo Fisher Scientific). Following four freeze-thaw cycles and sonication, lysates were cleared by centrifugation. The supernatant was incubated with glutathione- Sepharose 4B (17075601; GE) for 4 hours at 4°C. Following six washes with washing buffer (PBS 1X and 1% Triton) and with PBS 1X, Ocn was then cleaved out from the GST moiety by using thrombin (27-0846-01; GE). Four fractions were collected, and each of them was incubated with benzamidine Sepharose (17-5123-10; GE) for 30 min at room temperature to remove thrombin. 10ng (diluted in PBS 1X) of Ocn were injected per hemisphere in 16 month-old mouse hippocampi. Primary hippocampal neurons were treated with Ocn at a concentration of 10ng/ml of culture medium.

Osmotic pumps

Alzet micro-osmotic pumps (model 1002) were loaded with saline or uncarboxylated Ocn (30ng/hr). Mice were anesthetized with isoflurane and osmotic pumps were surgically installed subcutaneously in the backs of the mice. Behavioral analyses started 1 week after Osmotic pumps installation.

Primary cultured hippocampal neurons

Hippocampal neurons were isolated from mouse embryos (embryonic day 16.5). After dissection, hippocampi were digested with trypsin 0.05% and EDTA 0.02% for 15 min at 37°C. After three washes with DMEM (61965059: Thermo Fisher Scientific) supplemented with 10% FBS, 100 U/ml penicillin-streptomycin and 1x GlutaMAX (Thermo Fisher Scientific), cells were dissociated by pipetting up and down, and then plated. The dissociated cells were plated onto poly-L-lysine-coated plates or glass coverslips for microscopic examination. 24h after plating, the media was replaced with Neurobasal medium (Thermo Fisher Scientific) containing B27 supplement (Thermo Fisher Scientific), GlutaMAX and Mycozap (Lonza) was changed two times per week and neurons were maintained in 5% CO2 and 37°C. Experiments were performed on cells after 15 days of culture.

Neuronal stimulation treatment of primary hippocampal neurons

For chemical long-term potentiation (cLTP), primary hippocampal neurons (DIV15) were treated as described by Oh and Derkach [51] and then incubated for 2 hr with neurobasal medium containing or not 100mM bafilomycin A1 (Baf). For KCl depolarization, neurons were pretreated with neurobasal medium containing 60nM KCl for 10 min and then incubated for 2 hr with neurobasal medium containing or not 100mM Baf. For Ocn, neurons were treated for 4 hr with neurobasal medium containing either 10ng/ml Ocn, 100mM Baf or both. For bafilomycin A1 (Baf) treatment, neurons were treated with neurobasal medium containing 100mM Baf either for 2 hr (cLTP and KCl treatments) or for 4 hr (Ocn treatment). After treatment, neurons were rinsed in PBS and proteins extracted in 1X Laemmli buffer containing phosphatase and protease inhibitors.

Lentiviral infections and transfection of primary hippocampal neurons

Primary hippocampal neurons were infected (MOI5) at Day *In Vitro* (DIV) 1 with lentiviruses (pLKO-IPTG-3XLacO) expressing an IPTG (Isopropyl β-D-1-thiogalactopyranoside)-inducible shRNA targeting mouse Beclin-1 (*Becn 1*) (Sigma-Aldrich): 5′-TGC GGG AGT ATA GTG AGT TTA ATT CAA GAG ATT AAA CTC ACT ATA CTC CCG CTT TTT TC-3′ (sense); 3′- TCG AGA AAA AAG CGG GAG TAT AGT GAG TTT AAT CTC TTG AAT TAA ACT CAC TAT ACT CCC GCA-5′(anti-sense). The same lentiviral plasmid construct together with a plasmid expressing EGFP were also used to co-transfect neurons at DIV11 with Lipofectamine 2000 (Thermo Fischer Scientific) following manufacturer's instructions, to study dendritic spines density. Infected or transfected neurons were treated with 5mM IPTG for 72 hours to induce shRNA-*Beclin-1* expression. Neurons were then treated at DIV15 as described below.

Dendritic spines density analysis *in vitro*

Neurons were fixed 1 hour after cLTP induction in 4% PFA /4% glucose for 20 min at room temperature. The coverslips were then washed 3 times in PBS and mounted with Fluoromount Aqueous Mounting Medium. LacI (Millipore) detection by immunofluorescence was carried out to identify EGFP and *Beclin 1*-shRNA co-transfected neurons. Fluorescence images of LacI and EGFP positive neurons were obtained using a Zeiss Apotome2 (40X objective). Dendritic spine density was analyzed using NeuronStudio software. For each neuron, spines from two distinct secondary and tertiary dendrite segments were counted. 16 neurons from 4 biological replicates were analyzed for each group. Blind analyses were performed by two independent investigators.

Golgi Cox Staining and dendritic spines quantification

3 month-old treated mice were intracardially perfused with 4% PFA and the isolated brains were subjected to Golgi impregnation using FD Rapid GolgiStain Kit (FD Neuro Technologies, Baltimore, MD) following manufacturer's instructions. Bright field z stacks of 100 μm sections were obtained using a Zeiss Apotome2 (40X objective). Dendritic spine density was quantified manually (NeuronJ software, https://imagescience.org/meijering/software/neuronj/). For each mouse group, 4 secondary dendrite segments from 20-30 of dentate gyrus granule cells were quantified. The analysis was performed blinded by three independent investigators.

TUNEL Assay

To assess apoptosis in mouse brains after hippocampal stereotactic injections of AAV expressing shRNA (3 weeks post injections) or pharmacological autophagy modulator (TAT-Beclin 1, Spautin 1, Leupeptin and Chloroquine) (24 hours post injections), 30 μm cryostat sections were processed using the ApopTag® Peroxidase Direct *In Situ* Apoptosis Detection Kit (Millipore) according to manufacturer's protocol. Images were obtained using Nanozoomer 2.0 (Hamamatsu) and the number of apoptotic cells was evaluated on 14 serial hippocampal sections (30 μm) for each mice.

Electrophysiology

Ex vivo slice preparation

Brain slices were prepared from 3 months-old Swiss mice from Janvier (Le Genest St Isle, France). The brain was removed quickly and 350 μm thick sagittal slices containing both cortex and hippocampus were cut in ice-cold sucrose solution (in mM: KCl 2.5, NaH_2PO4 1.25, $MgSO_4$ 10, $CaCl_2$ 0.5, NaHCO3 26, Sucrose 234, and Glucose 11, saturated with 95% O2 and 5% CO2) with a Leica VT1200 blade microtome (Leica Microsystemes, Nanterre, France). After the cutting, hippocampus was extracted from the slice and transferred in oxygenated ACSF (in mM: NaCl 119, KCl 2.5, NaH_2PO_4 1.25, $MgSO_4$ 1.3, $CaCl_2$ 2.5, $NaHCO_3$ 26, and Glucose 11) at 28 ± 1°C for 30 minutes and then incubated and kept at room temperature for 1 hour with either vehicle or spautin-1 (10 μM) before and during recordings.

Electrophysiological recordings

Each slice was individually transferred to a submersion-type recording chamber and continuously superfused (2ml/min) with oxygenated ACSF. Extracellular recordings were obtained at 28°C from the apical dendritic layers of the hippocampal CA1 area, using glass micropipettes filled with ACSF. Field excitatory postsynaptic potentials (fEPSPs) were evoked by the electrical stimulation of Schaeffer collaterals afferent to CA1. The magnitude of the fEPSPs was determined by measuring their slope. Signals were acquired using a double EPC 10 Amplifier (HEKA Elektronik Dr. Schulze GmbH, Germany) and analyzed with Patchmaster software (HEKA Elektronik Dr. Schulze GmbH, Germany).

Input/output (I/O) curves. The slope of fEPSPs was plotted as a function of stimulation intensity (0 to 100 μA). In control condition 7 slices from 4 mice were used and 6 slices from 3 mice in spautin condition.

Paired-pulse facilitation (PPF). PPF of synaptic transmission was induced by paired stimulation with different inter-stimulus interval from 25 to 300 ms. PPF was quantified by normalizing the magnitude of the second response to the magnitude of the first one. In control condition 8 slices from 4 mice were used and 8 slices from 4 mice in spautin-1 condition.

Long-term potentiation (LTP). Test stimuli were delivered once every 15 s and the stimulus intensity was adjusted to produce 40%–50% of the maximal response. A stable baseline was recorded for at least 15min. LTP was induced by Theta Burst Stimulation (TBS involved 5 trains with 10 bursts of 4 pulses delivered at 100 Hz, an interburst interval of 200 ms and 20 s interval between each train). Average value of fEPSP slope was expressed as a percentage of the baseline response ± SEM. In control condition 7 slices from 7 mice were used and 7 slices from 4 mice in spautin condition. Results are expressed as the mean ± SEM from independent biological samples. Statistical analyses were performed with GraphPad Prism 6.0. (RRID:SCR_015807). I:O curve, PPF and LTP were analyzed by non-parametric Mann-Whitney U test, p values are indicated in the corresponding figure legend (i.e., ns = not significant, *$p < 0.05$, ***$p < 0.001$).

QUANTIFICATION AND STATISTICAL ANALYSIS

All values are expressed as mean ± s.e.m. Alpha was set to 0.05 for all analyses. Statistical parameters including the exact sample size (n), post hoc tests, and statistical significance are reported in every figure and figure legend. Number of mice was estimated to be sufficient on the basis of pilot experiments. Data were estimated to be statistically significant when $p \leq 0.05$ by nonparametric

Mann-Whitney U test or Student's t test, and one-way or two-way ANOVAs with repeated-measures when appropriate. Significant ANOVAs were followed by a two-way repeated-measures analysis of variance with a post hoc Tukey's HSD multiple comparisons test for pairwise differences between each mouse groups. In every figure, an asterisk denotes statistical significance (*, $p \leq 0.05$; **, $p \leq 0.01$; ***, $p \leq 0.001$). Data were analyzed using GraphPad Prism v5 software.

DATA AND SOFTWARE AVAILABILITY

Data resources

All software used in this manuscript is listed the Key Resources Table.